Research Article

Nerve bundle formation during the promotion of peripheral nerve regeneration: collagen VI-neural cell adhesion molecule 1 interaction

https://doi.org/10.4103/1673-5374.324861
Date of submission: February 22, 2021
Date of decision: April 24, 2021
Date of acceptance: May 29, 2021
Date of web publication: September 17, 2021

Jia-Hui Sun[1, 2, #], Ming Huang[3, #], Zhou Fang[2], Tian-Xiao Li[4], Ting-Ting Wu[2], Yi Chen[3], Da-Ping Quan[5], Ying-Ying Xu[2], Yu-Ming Wang[1, 2], Yi Yang[6, *], Jian-Long Zou[1, 2, *]

Graphical Abstract *COL6 promotes nerve bundle formation through immobitization of NCAM1 on axolemma*

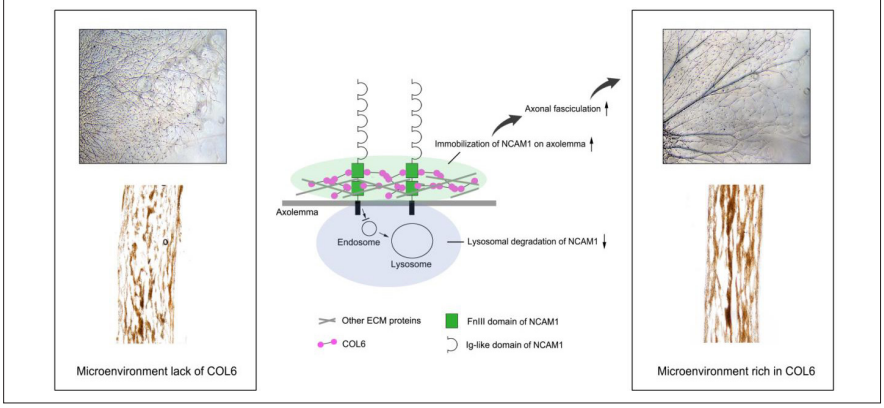

Abstract

The formation of nerve bundles, which is partially regulated by neural cell adhesion molecule 1 (NCAM1), is important for neural network organization during peripheral nerve regeneration. However, little is known about how the extracellular matrix (ECM) microenvironment affects this process. Here, we seeded dorsal root ganglion tissue blocks on different ECM substrates of peripheral nerve ECM-derived matrix-gel, Matrigel, laminin 521, collagen I, and collagen IV, and observed well-aligned axon bundles growing in the peripheral nerve ECM-derived environment. We confirmed that NCAM1 is necessary but not sufficient to trigger this phenomenon. A protein interaction assay identified collagen VI as an extracellular partner of NCAM1 in the regulation of axonal fasciculation. Collagen VI interacted with NCAM1 by directly binding to the FNIII domain, thereby increasing the stability of NCAM1 at the axolemma. Our *in vivo* experiments on a rat sciatic nerve defect model also demonstrated orderly nerve bundle regeneration with improved projection accuracy and functional recovery after treatment with 10 mg/mL Matrigel and 20 μg/mL collagen VI. These findings suggest that the collagen VI-NCAM1 pathway plays a regulatory role in nerve bundle formation. This study was approved by the Animal Ethics Committee of Guangzhou Medical University (approval No. GY2019048) on April 30, 2019.

Key Words: axonal fasciculation; collagen VI; extracellular matrix; microenvironment; nerve bundle formation; nerve projection; neural cell adhesion molecule 1; neurogenesis; peripheral nerve regeneration

Chinese Library Classification No. R446; R741; R318

Introduction

Peripheral nerves have a remarkable ability to regenerate (Cattin and Lloyd, 2016; He et al., 2016; Raza et al., 2020). However, functional recovery from severe peripheral nerve injury, such as nerve defects, remains limited because regenerated nerve fibers are apt to grow diffusely and fail to maintain the fasciculated structure of the original nerve bundles (English, 2005; de Ruiter et al., 2014).

Many cell adhesion molecules (CAMs) have been discovered in nervous tissues that mediate axon growth behaviors during

[1]Institute of Neuroscience and the Second Affiliated Hospital of Guangzhou Medical University, Key Laboratory of Neurogenetics and Channelopathies of Guangdong Province and the Ministry of Education of China, Guangzhou, Guangdong Province, China; [2]Key Laboratory of Neurological Function and Health, School of Basic Medical Sciences, Guangzhou Medical University, Guangzhou, Guangdong Province, China; [3]Zhongshan School of Medicine, Sun Yat-sen University, Ministry of Education, Guangzhou, Guangdong Province, China; [4]Department of Pharmacy, Hospital of Stomatology, Guanghua School of Stomatology, Sun Yat-sen University, Guangzhou, Guangdong Province, China; [5]Key Laboratory for Polymeric Composite and Functional Materials of Ministry of Education, School of Chemistry, Sun Yat-sen University, Ministry of Education, Guangzhou, Guangdong Province, China; [6]Department of Orthopedic Trauma and Microsurgery, The First Affiliated Hospital, Sun Yat-sen University, Guangzhou, Guangdong Province, China
*Correspondence to: Jian-Long Zou, MD, zou_jianlong@gzhmu.edu.cn; Yi Yang, MD, yangy523@mail.sysu.edu.cn.
https://orcid.org/0000-0002-1401-4628 (Jian-Long Zou); https://orcid.org/0000-0002-0692-8024 (Yi Yang); https://orcid.org/0000-0002-8163-558X (Jia-Hui Sun)
#Both authors contributed equally to this work.

Funding: *This study was supported by the National Natural Science Foundation of China, No. 31800892 (to JLZ); the Natural Science Foundation of Guangdong Province of China, No. 2018A030310254 (to YY); and a grant from Guangzhou Medical University Start-up Project of China, No. B195002002048 (to JLZ).*
How to cite this article: *Sun JH, Huang M, Fang Z, Li TX, Wu TT, Chen Y, Quan DP, Xu YY, Wang YM, Yang Y, Zou JL (2022) Nerve bundle formation during the promotion of peripheral nerve regeneration: collagen VI-neural cell adhesion molecule 1 interaction. Neural Regen Res 17(5):1023-1033.*

development and neuronal injury (Van Vactor, 1998; Chen et al., 2019; Chooi and Chew, 2019; Elazar et al., 2019; Mathot et al., 2021; Yuan et al., 2021). Among these molecules, neural cell adhesion molecule 1 (NCAM1) is involved in the fasciculation of axons (Rutishauser et al., 1988; Lin et al., 1994; Cremer et al., 1997; Fujita et al., 2000). Because of alternative transcript splicing, there are three main NCAM1 isoforms, NCAM180, NCAM140, and NCAM120, in the nervous system. These isoforms share an identical extracellular domain that consists of five N-terminal Ig-like domains (Ig I–V) followed by two fibronectin type III domains (FN3, I and FN3, II) (Cunningham et al., 1987). The Ig domains provide NCAM1 with homophilic (NCAM-NCAM) binding activity, and the FN3 domains enable heterophilic interactions between NCAM1 and other molecules (Cunningham et al., 1987; Carafoli et al., 2008; Eggers et al., 2011). These interactions activate a series of signaling cascades, such as mitogen-activated protein kinase-, extracellular signal-regulated kinase-, p21-activated kinase 1-, and focal adhesion kinase-dependent pathways, thereby mediating neuronal migration, adhesion, neurite outgrowth, and axonal fasciculation (Crossin and Krushel, 2000; Kolkova et al., 2000; Li et al., 2013). Based on these findings, many NCAM1 mimetic peptides have been developed to promote neurite outgrowth and perform neuroprotective functions (Neiiendam et al., 2004; Chu et al., 2018).

In addition to CAMs, a variety of extracellular matrix (ECM) components have been shown to act as environmental (extrinsic) signals that affect nerve regeneration processes such as axon growth, myelinization, synapse formation, and axon guidance (Giger et al., 2010; Gonzalez-Perez et al., 2013; de Luca et al., 2014; Ferrer-Ferrer and Dityatev, 2018; Zou et al., 2018). As an ECM component, collagen VI (COL6) is broadly distributed at the interface between the basement membrane and interstitial matrix in various tissues (Groulx et al., 2011). Through its interactions with different ECM components and CAMs, COL6 has the ability to bridge cells to the surrounding connective tissue and modulate the stiffness and other mechanical properties of the ECM (Urciuolo et al., 2013). Recent studies have also revealed the roles of COL6 in regulating several intracellular pathways, such as that involved in apoptosis (Cescon et al., 2016), tumor progression (You et al., 2012), myelination (Chen et al., 2014), and macrophage polarization (Chen et al., 2015). However, the COL6-NCAM1 interactions in the nervous system, along with the regulatory mechanisms of COL6 that are linked to axonal fasciculation, are unknown.

In our previous study, we created a decellularized nerve matrix-gel (DNM-G) consisting of sciatic nerve ECM (Zou et al., 2018). We observed a unique phenomenon whereby axons of dorsal root ganglia (DRG) tended to gather into large bundles when grown in the peripheral nerve ECM environment of DNM-G. We hypothesized that the enhanced axonal fasciculation in DNM-G is caused by some key ECM component that improves the function of NCAM1. To test this hypothesis, we investigated the role of NCAM1 in nerve bundle formation. By performing co-immunoprecipitation with NCAM1 as bait to elicit interactions with the components of DNM-G, we further identified the key ECM component that contributes to the formation of nerve bundles during peripheral nerve regeneration.

Materials and Methods

Animals

After spinal cord or sciatic nerve injury, male rats are more likely to gnaw their denervated legs, causing infection and death (Wagner et al., 1995). Therefore, female rats are preferred in these nerve injury models. Neonatal (3–5 days postnatal, random sex, 10–12 g) and adult (60 days postnatal, female, ~220 g) Sprague-Dawley rats were purchased from the Animal Center Laboratory of Sun Yat-sen University (license No. SCXK (Yue) 2016-0029). Two male and two female miniature pigs (8 months old, 8–10 kg) were supplied by the Animal Center Laboratory of Southern Medical University (license No. SCXK (Yue) 2016-0041). All rats were housed under specific pathogen-free conditions at a temperature of 22 ± 1°C, and all pigs were housed under conventional conditions at a temperature of 26 ± 2°C. All animal experiments in this study were carried out in accordance with the ethical standards of the Animal Ethics Committee of the Guangzhou Medical University (approval No. GY2019048) on April 30, 2019.

Preparation of DNM-G

The preparation of DNM-G has been detailed in a previous publication (Zou et al., 2018). In brief, the miniature pigs were sacrificed under deep anesthesia, and sciatic nerve tissues were immediately collected. Cellular components were sequentially extracted using Triton X-100 (3%), sodium deoxycholate (4%), and sterile water washes at 4°C. De-fat and freeze-drying processes were performed before the tissues were homogenized into powder, and pepsin was used to digest the powder for 12 hours at 25°C. Any undigested particles were removed by centrifugation. The solution pH was adjusted to 7.5, and the ionic strength was set at 0.15 M using 10× phosphate buffer saline (PBS). Then, the pregel solution was aliquoted and stored at –20°C until use.

Coating of cell culture plate

Pregel DNM-G and Matrigel (Corning, Corning, NY, USA, Cat# 356230, growth factor reduced) solutions were stored at –20°C and thawed at 4°C before use. We added cold Neurobasal-A medium (Thermo Fisher Scientific, Waltham, MA, USA, Cat# 10888022) to an aliquot of DNM-G or Matrigel to make a 1 mg/mL protein solution. The diluted solution was added to culture plates at 200 μg/cm^2, placed at 37°C for 2 hours, and washed with PBS before seeding the DRGs. For the collagen coating, a COL1 stock solution (rat native, Corning, Cat# 354236), or COL6 stock solution (human native, Corning, Cat# 354261) was diluted with cold Neurobasal-A medium to obtain a 20 μg/mL solution. The solution was added to the culture dishes at 1 μg/cm^2 and evenly applied to cover the entire bottom. Next, the culture dishes were placed at 37°C for 2 hours and washed once before introducing the cells and medium. For laminin, laminin 521 stock solution (human recombinant, BioLamina, Sundbyberg, Sweden, Cat# LN521) was slowly thawed at 4°C prior to use. We diluted the stock solution with Neurobasal-A medium to generate a 10 μg/mL solution and added this to the dishes at 2 μg/cm^2. The dishes were incubated at 4°C overnight and washed once before use.

In some experiments, COL6 (Corning, Cat# 354261) and Matrigel were concurrently dissolved in cold Neurobasal-A medium to make a series of mixed solutions containing 1 mg/mL Matrigel and gradient concentrations of COL6 (4, 20, and 100 μg/mL). The mixed COL6 and Matrigel solutions were applied to the bottoms of culture plates using the same procedure described for the Matrigel solution. The plates coated with the mixed COL6 and Matrigel solution were termed the Matrigel + COL6 group; plates coated with a solution containing 20 μg/mL COL6 and a vehicle (Neurobasal-A medium, applied following the same procedure used for the collagen coating) were termed the COL6 + Vehicle group; and plates precoated with a solution containing 1 mg/mL Matrigel and vehicle (applied following the same procedure used for the Matrigel coating) were termed the Matrigel + Vehicle group.

DRG *ex vivo* preparation

Rats (3–5 days postnatal, random sex) were deeply anesthetized intraperitoneally with pentobarbital (200 mg/kg,

Sigma-Aldrich, San Francisco, CA, USA). Next, DRGs were dissected and collected in cold Neurobasal-A medium. The redundant nerve roots and epineurium were completely removed under a stereomicroscope (Sunny Optical, Ningbo, China). The DRGs were transferred into protein-precoated dishes and cultured with Neurobasal-A medium containing 2% B27 (Gibco, Grand Island, NY, USA, Cat# 17504044), 0.5 mM L-glutamine (Gibco, Cat# 25030081), and 50 ng/mL recombinant human β-nerve growth factor (Peprotech, Rocky Hill, NJ, USA, Cat# 450-01) in a 37°C incubator with 5% CO_2 and 92% humidity. The medium was changed every other day.

Culture of primary DRG neurons

After the residual roots had been trimmed, the DRG tissue blocks were incubated with 0.25% trypsin (Sigma-Aldrich, Cat# T4049) at 37°C for 15 minutes and then dissociated by pipetting the solution up and down 200 times. The cells were pelleted via centrifugation at 200 × *g* for 1 minute. The supernatant was discarded and the cell pellets were resuspended in Neurobasal-A culture medium containing 2% B27, 0.5 mM L-glutamine, and 50 ng/mL recombinant human β-nerve growth factor. Cells in suspension were seeded on protein-precoated 24-well dishes at a density of 1.0×10^5 cells/well and incubated in a 37°C incubator with 5% CO_2 and 92% humidity. The medium was changed every other day.

Co-culture of DRG and Schwann cells

DRGs were dissected from rats with ~0.5 mm roots retained. The rest of the steps were the same as for the primary DRG neuron culture, as described above.

Immunofluorescence staining

After 72 hours of incubation, the DRG tissue blocks or DRG neurons were fixed in 4% paraformaldehyde for 2 hours, rinsed three times with PBS for 30 minutes each time, permeabilized, and blocked with 0.3% Triton X-100 (Sigma-Aldrich, Cat# T8787) and 10% normal goat serum (Invitrogen, Waltham, MA, USA, Cat# 31873) in PBS for 30 minutes. The specimens were then incubated with anti-NCAM1 antibody (1:300, rabbit monoclonal, Abcam, Cambridge, MA, USA, Cat# ab220360) and anti-neurofilament 200 antibody (axonal marker, NF200, 1:200, mouse monoclonal, Sigma-Aldrich, Cat# SAB4200705), followed by Cy3-conjugated goat anti-rabbit IgG (1:500, Beyotime, Shanghai, China, Cat# A0516) and Alexa Fluor 488-conjugated goat anti-mouse IgG (1:500, Beyotime, Cat# A0428) to visualize NCAM1 on axolemma. Nuclei were stained with 4′,6-diamidino-2-phenylindole (DAPI; Thermo Fisher Scientific, Cat# D1306). An anti-COL6 antibody (1:300, rabbit monoclonal, Abcam, Cat# ab182744) and CY3-conjugated goat anti-rabbit IgG (1:500, Beyotime, Cat# A0516) were used for immunofluorescence staining of COL6. The anti-S100 antibody (1:300, rabbit monoclonal, Abcam, Cat# ab136629) and Cy3-conjugated goat anti-rabbit IgG (1:500, Beyotime, Cat# A0516) were used for immunofluorescence staining of Schwann cells. All of the primary antibodies described above were incubated at 37°C for 3 hours and the secondary antibodies were incubated at 37°C for 1 hour.

Lysosome staining

Cells from DRG grown on 24-well plates were transfected with the Lysosomes-Green Fluorescent Protein BacMam 2.0 reagent (3 μL per well, Thermo Fisher Scientific, Cat# C10596) and incubated overnight before fluorescence microscopy (Nikon, Tokyo, Japan).

Transmission electron micrography

DRG tissue blocks cultured in DNM-G or Matrigel precoated dishes were scraped off after 5 days of incubation and pelleted via centrifugation at 500 × *g* for 5 minutes. The pellets were fixed and embedded in EPON-812, and then subjected to ultramicrotomy. After lead-uranium staining, the ultrathin sections were mounted and assessed using a transmission electron microscope (Philips XL30 FEG, Philips, Eindhoven, The Netherlands).

Analysis of axon bundle diameters

In a subset of DRG *ex vivo* cultures, diameters of single axons/axon bundles located ~1 mm from the center of the DRG tissue block were measured under a 40× objective lens. We counted the number of single axons/axon bundles with diameters larger than 3 μm, between 1 and 3 μm, and thinner than 1 μm, respectively; and then analyzed the distribution of axon diameters in terms of percentages.

Proteomic analysis

DNM-G-treated DRGs and Matrigel-treated DRGs were collected (n = 3 biological replicates) and lysed in a solution containing two volumes of L3 buffer (50 mM Tris-Cl, pH 8, 7 M urea, 2 M thiourea, and 1× protease inhibitor cocktails), eight volumes of ice-cold acetone, and 10 mM dithiothreitol. After tryptic digestion, the peptide samples were dissolved in 2% acetonitrile/0.1% formic acid and analyzed using high-resolution liquid chromatography-mass spectrometry/mass spectrometry (TripleTOF 5600+ mass spectrometer, SCIEX, Ramingham, MA, USA) coupled with an Eksigent nanoLC System (SCIEX). The original MS/MS file data were submitted to ProteinPilot Software v4.5 (SCIEX) for protein identification based on the UniProt database (https://www.uniprot.org/#). We used Skyline v3.6 software (SCIEX) for peptide and protein quantification. The fold-changes of the proteins were calculated as the average of comparison pairs (DNM-G/Matrigel) among biological replicates. Proteins with fold changes > 1.5 and $P < 0.05$ were considered to be significantly differentially expressed.

Gene ontology annotation

The gene ontology annotation protocol has been detailed in a previous publication (Sun et al., 2020). Briefly, the identified protein sequences were mapped via a homology search using the uniprot_sus database at http://geneontology.org. The e-value was set to less than $1 \times e^{-5}$, and the best hit for each query sequence was selected for gene ontology term matching. In this study, the annotation of "extracellular matrix" as a key word was set as the requirement for protein screening.

Western blot assay

Cultured DRGs were lysed in a radio immunoprecipitation assay buffer (Sigma-Aldrich, Cat# R0278) containing 1% protease/phosphatase inhibitor cocktail (Cell Signaling Technology, Danvers, MA, USA, Cat# 5872S). We measured the protein concentration using a bicinchoninic acid protein assay (Beyotime, Cat# P0009). Protein lysates were mixed with sodium dodecyl sulfate polyacrylamide gel electrophoresis loading buffer (Beyotime, Cat# P0015) and heated in a boiling water bath for 3 minutes. The protein samples were then loaded into sodium dodecyl sulfate-polyacrylamide gels (Bio-Rad, Hercules, CA, USA, Cat# 4568123). After electrophoresis and transfer, the membrane was blocked with QuickBlock™ Western blocking buffer (Beyotime, Cat# P0252) while being shaken for 10 minutes. A anti-NCAM1 antibody (1:1000, rabbit monoclonal, Abcam, Cat# ab220360) was used for incubation of the rat samples. Another anti-NCAM1 antibody (1:500, mouse monoclonal, Abcam, Cat# ab9018) was used for human recombinant NCAM120 detection. An anti-His antibody (1:1000, mouse monoclonal, Beyotime, Cat# AF5060) was used to detect recombinant protein with a His-tag. For COL6 immunoblotting, the membrane was incubated with an anti-COL6A1 antibody (1:2000, rabbit monoclonal, Abcam, Cat# ab182744). All of the primary antibodies

described above were incubated overnight at 4°C on a rotating shaker. After washing the membrane with Tris buffered saline-Tween 20 (Thermo Fisher Scientific, Cat# 28360), it was incubated with horseradish peroxidase-conjugated goat anti-mouse IgG (1:1000, Beyotime, Cat# A0216) or goat anti-rabbit IgG (1:1000, Beyotime, Cat# A0208) for 1 hour at room temperature. The protein bands were detected via electrochemiluminescence with a Chemiluminescence Imaging System (JS-M6, Peiqing Science and Technology, Shanghai, China). The protein expression levels were quantified using Image Lab software (version 6.0, Bio-Rad). The proteins of interest were normalized to β-actin (1:1000, mouse monoclonal, Beyotime, Cat# AA128), unless otherwise stated. We referred to the protein ladder for the molecular weights (Thermo Fisher Scientific, Cat# 26625).

Detection of total protein bands

Total protein bands were detected using Tris-Glycine eXtended Stain-Free technology. In brief, protein samples were loaded in a Tris-Glycine eXtended Stain-Free Precast Gel (Bio-Rad, Cat# 4568123). After electrophoresis, the total protein bands were imaged using a ChemiDoc MP imaging System (Bio-Rad). For the decellularized tissue samples, this method was also used to normalize the proteins of interest according to the total protein.

Antibody blocking assay

To disrupt the function of NCAM1 or COL6, DRGs seeded on the ECM-precoated dishes were treated with anti-NCAM1 antibody (1:500 diluted in the culture medium, Abcam, Cat# ab220360) at 37°C for 48 hours. Next, the DRGs were fixed and examined via microscope. DRGs treated with an anti-glyceraldehyde-3-phosphate dehydrogenase (GAPDH) antibody (1:500, rabbit monoclonal IgG, Beyotime, Cat# AF1186) were set as the control group.

NCAM1 plasmid transfection

In a subset of the primary DRG neuron cultures, the cells were transfected with NCAM1 cDNA (NM_031521.1) in expression vectors (Sino Biological, Cat# RG80399-UT) and the null-vectors (Sino Biological, Cat# CV011) were used as normal controls (NC). In brief, transfection was performed immediately after seeding the cells on dishes. Lipofectamine 3000 reagent (Thermo Fisher Scientific, Cat# L3000008) was diluted 3:50 in Opti-MEM medium (Gibco, Cat# 11058021). The master mix of DNA was prepared by diluting 1 μg of DNA in 52 μL Opti-MEM medium containing 2 μL P3000 reagent. Next, the diluted DNA was mixed with the diluted Lipofectamine 3000 reagent at a 1:1 ratio and incubated for 10 minutes at room temperature to form the DNA-lipid complex. For the 24-well plate, 50 μL of the DNA-lipid complex was added to each well. Cells were normally incubated for 3 days, followed by immunofluorescence staining as described above.

Co-immunoprecipitation

After 2 days of incubation, the DRGs growing on the DNM-G-coated substrate were collected and lysed in native lysate buffer (Invent Biotechnologies, Cat# SN-002) containing 1% protease/phosphatase inhibitor cocktail (Cell Signaling Technology, Cat# 5872S). The lysate was then centrifuged at 5000 × *g* and 4°C for 5 minutes. The supernatant was collected for a subsequent immunoprecipitation assay conducted using the Dynabeads™ Protein A Immunoprecipitation Kit (Thermo Fisher Scientific, Cat# 10006D). The following steps were performed according to the manufacturer instructions. In brief, 5 μg anti-NCAM1 antibody (Abcam, Cat# ab220360) or 5 μg anti-COL6 antibody (Abcam, Cat# ab6588) was incubated with 1.5 mg Dynabeads in the Ab Binding & Washing Buffer to form the Dynabeads-Ab complex. For the NC, the Dynabeads were incubated in vehicle without an antibody. The Dynabeads-Ab complex was then mixed with protein lysate (2 mg of protein) and incubated for 10 minutes at room temperature with rotation to form the Dynabeads-Ab-Ag complex. The uncombined proteins were removed via thorough washing with washing buffer. Proteins in the Dynabeads-Ab-Ag complex were eluted using the elution buffer, followed by immunoblotting detection as described above.

Recombinant protein expression and purification

The DNA segment encoding the extracellular region of Ig-like domains (Leu20 to Val495) and that encoding the extracellular region of FnIII domains (Gln496 to Gly740) of human NCAM120 were inserted between the BglII and XhoI sites of the mammalian expression system vector proEM™ (DetaiBio, Nanjing, China) and connected to a C-terminal His6 tag, respectively. The recombinant proEM™ vectors were first amplified in DH5α cells and then used to infect HEK293 cells (American Type Culture Collection, Manassas, VA, USA) to produce soluble NCAM (20–495) and NCAM (496–740) proteins. The secreted proteins were collected from the medium using nickel-nitrilotriacetic acid affinity chromatography and then purified using a Superdex 75 column (GE Healthcare, Boston, MA, USA). The purified proteins were concentrated to 1.5 mg/mL in 1 × PBS and 10% glycerol (pH 7.4).

Quantitative real-time polymerase chain reaction

After culturing the DRGs for 3 days, the total RNA of the DRGs was extracted using the Trizol method. For reverse transcription, a PrimeScript™ RT reagent kit (Takara, Kusatsu, Shiga, Japan, Cat# RR047A) was used to synthesize cDNA. Next, a quantitative polymerase chain reaction was performed in triplicate using the 7900HT Fast Real-Time Polymerase Chain Reaction System (Thermo Fisher Scientific) and PowerUp™ SYBR Green mix (Thermo Fisher Scientific, Cat# A25742). Primers (forward: 5′-TTC CTG TGT CAA GTG GCA GG-3′, reverse: 5′-TAA ACT CCT GTG GGG TTG GC-3′) were used to determine the mRNA levels of rat *Ncam1*. *Gapdh* was used as a reference for normalization (forward: 5′-GTC GGT GTG AAC GGA TTT GG-3′ and reverse: 5′-ACG ACA TAC TCA GCA CCA GC-3′). SDS 2.4 software (Thermo Fisher Scientific) was used to analyze the quantitative polymerase chain reaction data. The mRNA levels of *Ncam1* relative to the mRNA levels of the reference gene *Gapdh* were calculated.

Preparation of the sciatic nerve defect model and repair

Female rats were anesthetized with isoflurane (4%, 0.6 L/min; 2 minutes for induction and 2% for maintenance, RWD, Shenzhen, China) using a R540 Small Animal Anesthesia Machine (RWD). The right sciatic nerve was exposed at the mid-thigh level, and the adhering fascia between the biceps femoris muscles and gluteus was freed. The sciatic nerve was transected, and approximately 8 mm of the distal stump was removed. The damaged stumps were bridged with a hydrogel-filled silicone catheter (1.2 mm in diameter, Merck, Darmstadt, Germany) using a 10-0 monofilament nylon suture. In the M + V group, the catheter was filled with 10 mg/mL Matrigel + Vehicle (Neurobasal-A medium). In M + C group, the catheter was filled with 10 mg/mL Matrigel + 20 μg/mL COL6. An empty catheter filled with saline was used for the negative control (E group).

Silver staining of sciatic nerve regeneration

After 8 weeks of recovery, the rats with a sciatic nerve defect were sacrificed via an overdose of isoflurane anesthesia (5%, 3 L/min; 3–5 minutes). Sciatic nerves were dissected and fixed in 4% paraformaldehyde for 48 hours followed by sucrose dehydration and cryo-section (20-μm thickness). Longitudinal sections of the sciatic nerve were stained using Bielschowsky's

nerve staining kit (Leagene Biotechnology, Beijing, China, Cat# DK0015). In brief, the sections were washed with distilled water and immersed in silver nitrate solution for 10 minutes at 37°C away from light. The sections were briefly rinsed with distilled water for 2 minutes, and a 10% formalin solution was used to develop the silver stain for 1–3 minutes (until the section turned yellow). The sections were directly transferred into distilled water for 3–5 minutes and then placed into an ammoniacal silver solution for another 2 minutes followed by a 10% formalin reduction for 1 minute. After washing the sections in distilled water, the reaction was stopped via the application of 5% sodium thiosulfate for 5 minutes. The sections were then rinsed, dehydrated, cleared, and mounted for imaging.

Fluorescence tracing in the tibial nerve tract

The sciatic nerve with the tibial nerve branch was dissected from the rats and fixed in 4% paraformaldehyde for 24 hours. NeuroTrace® CM-DiI tissue-labeling paste (Invitrogen, Cat# N22883) was applied to the distal end of the tibial nerve using the tip of a needle. Tissues were kept at 4°C for 5 days, after which the proximal nerve trunk was cryo-sliced for fluorescence microscopy. The accuracy of the tibial nerve projection was calculated as the ratio of the integrated fluorescence density in the tibial nerve region and the integrated fluorescence density in the whole nerve stem.

Assessment of neurological function

At 2, 4, 6, and 8 weeks after the surgery, black ink was applied to the hind paws of the rats, and they were placed in a 10 cm × 40 cm corridor covered with a sheet of white paper. By measuring the consequent footprints, we obtained the parameters of print length (PL) and toe spread (TS) from both the normal side (N) and experimental side (E). The sciatic nerve function index was calculated using the following formula: sciatic nerve function index = 118.9 [(ETS – NTS)/ NTS] – 51.2 [(EPL – NPL) / NPL] – 7.5.

At 8 weeks after the surgery, the rats were anesthetized with isoflurane, and the right sciatic nerve was exposed. Stimulating electrodes were placed rostrally and caudally to the nerve conduit, and electrical stimuli were set at 8 V, 30 Hz. A recording electrode was placed in the gastrocnemius, enabling us to record and measure compound muscle action potential (CMAP) and the motor nerve conduction velocity using the Biology Function Laboratory System (BL-420, TECHMAN, Chengdu, China). The CMAP and the motor nerve conduction velocity of the contralateral normal nerve were regarded as the normal control.

Statistical analysis

All statistical tests and plots were performed using Prism 8 software (GraphPad, San Diego, CA, USA). Data are presented as the mean ± standard deviation (SD). Continuous variables were compared between the two groups using a Student's *t*-test if the data followed a normal distribution or a Wilcoxon-Mann-Whitney test if the data did not follow a normal distribution. Differences among three or more groups were compared using a one-way analysis of variance followed by Tukey's multiple comparison tests if the data followed a normal distribution, or a Kruskal-Wallis test followed by a Dunn-Bonferroni *post hoc* multiple comparison test if the data did not follow a normal distribution. A two-tailed *P*-value < 0.05 indicated statistical significance.

Results

Fasciculation of axons in the peripheral nerve ECM-derived environment

DNM-G was precoated at the bottom of the culture dishes, followed by DRG tissue seeding. Matrigel-precoated dishes were included as controls. After 72 hours of incubation, the axons growing on the DNM-G substrate were clustered into large bundles, whereas the Matrigel gave rise to dispersed and curved axons (**Figure 1A**). The axonal trajectories on the other ECM substrates (laminin 521, collagen I, and collagen IV) were also in a dispersed state (**Additional Figure 1**). Axon bundle diameter analyses (**Additional Figure 2**) showed that more than 20% of the axon bundles in the DNM-G were larger than 3 μm in diameter, an d that 40% were between 1 and 3 μm. In the Matrigel group, we detected no axon bundles larger than 3 μm; more than 80% of the axon bundles were less than 1 μm in diameter (*n* = 5 cultures, *P* < 0.0001, **Figure 1B**).

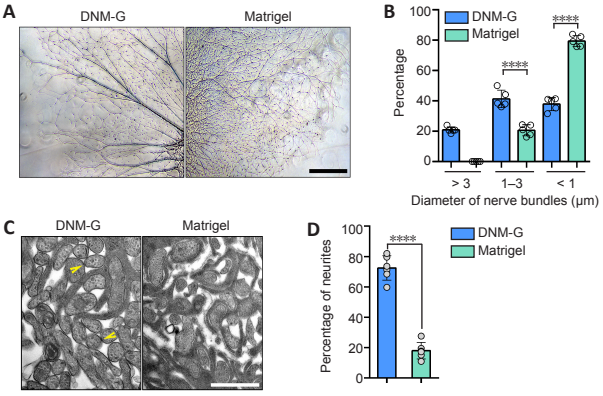

Figure 1 | Morphological analysis of axons in a peripheral nerve ECM-derived environment.

(A) DRG axons growing on different ECM substrates. The DNM-G substrate induced the formation of axon bundles, whereas the Matrigel gave rise to dispersed axons. (B) We compared the distribution of axon bundle diameters between DNM-G and Matrigel treated DRGs (*n* = 5 cultures, ****$P < 0.0001$, Student's *t*-test). (C) Electron microscopy of axons in DRG *ex vivo* preparations. There were more axonal contacts in the DNM-G group than in the Matrigel group. Arrowheads indicate contacts between axons. (D) Percentage of axons attached to one another in the DNM-G and Matrigel groups (*n* = 6 independent experiments, ****$P < 0.0001$, Student's *t*-test). Scale bars: 600 μm in A and 1 μm in C. DNM-G: Decellularized nerve matrix-gel; DRG: dorsal root ganglion; ECM: extracellular matrix.

The interactions between axons in transverse sections were examined via transmission electron microscopy. We found that there were more axons in contact with each other in the DNM-G group (72.42 ± 8.03%) than in the Matrigel group (18.01 ± 5.52%, *n* = 6 experiments, more than 90 axons were counted in each experiment, *P* < 0.0001, **Figure 1C** and **D**).

NCAM1 is involved in DNM-G-induced axonal fasciculation

CAMs are known to regulate a series of cell dynamics. Among them, NCAM1 was selected as the putative candidate owing to its role in regulating axonal fasciculation (Cunningham et al., 1987; Lin et al., 1994; Cremer et al., 1997). Immunoblotting confirmed the upregulation of three NCAM1 isoforms (NCAM180, NCAM140, and NCAM120) in DNM-G-treated DRGs compared with Matrigel-treated DRGs (*P* = 0.0063, **Figure 2A** and **B**). We also tracked dynamic changes in NCAM1 expression levels and found an increase in NCAM1 after DNM-G treatment, in contrast to a decrease after Matrigel treatment (*P* < 0.0001, **Additional Figure 3A** and **B**).

Consistent with the immunoblot results, immunofluorescence staining of both DRG *ex vivo* (**Figure 2C**) and DRG neuron cultures showed higher axonal NCAM1 fluorescence intensity in the DNM-G group compared with the Matrigel group (*P* < 0.0001, **Figure 2D** and **E**). However, the fluorescence intensity of NCAM1 in the DRG soma was not significantly different between the two groups (*P* = 0.4698, **Figure 2D** and **E**). These results indicate that the DNM-G-induced axonal fasciculation was correlated with the expression of NCAM1 in axons.

We blocked the function of NCAM1 using an antibody that specifically binds to its extracellular region. We used an IgG that binds to cytoplasmic GAPDH and has no biological function outside the cell as a negative control (**Figure 2F**). In comparison with the GAPDH antibody, the NCAM1 antibody treatment reduced the diameter of the axon bundles (**Figure 2G**). These data confirmed the role of NCAM1 in mediating axonal fasciculation.

Next, we tested whether overexpression of NCAM1 in Matrigel-treated DRGs could revise their axonal disorganization. DRG neurons growing on DNM-G and Matrigel substrates were transfected with NCAM1 cDNA. However, we found no improved axonal fasciculation in Matrigel after 3 days of culturing. We measured the fluorescence intensity of NCAM1 in the soma and axon regions. The results showed that in the DNM-G group, the NCAM1 plasmid transduction significantly increased the fluorescence intensity of NCAM1 in both the DRG soma and axons. In contrast, in the Matrigel group, the same treatment only increased NCAM1 in DRG somas, but not in axons ($P < 0.0001$, **Additional Figure 3C** and **D**).

Identification of COL6 as the extracellular signal for axonal fasciculation

Interactions between NCAM1 and ECM components are highly relevant to cytoskeletal rearrangements, and thereby modulate a range of biological processes, including cell adhesion and migration (Nielsen et al., 2010). To assess the presence of interactions between NCAM1 and DNM-G components, we performed co-immunoprecipitation in the DNM-G-DRG culturing system using NCAM1 as bait. Sodium dodecyl sulfate polyacrylamide gel electrophoresis showed several specific bands in the co-immunoprecipitation lanes (**Figure 3A**). High-resolution liquid chromatography-mass spectrometry/mass spectrometry identified the protein species in these bands. The proteins in the NCAM1-Ab solution and in the negative control (NC) were also found to exclude nonspecific binding proteins. We screened 17 proteins by analyzing the liquid chromatography-mass spectrometry/mass spectrometry data, and further reduced the number of protein candidates to five (COL1A2, COL6A1, COL6A2, LAMC1, and LAMB2) by selecting those belonging to the ECM (**Figure 3B**). These five protein monomer candidates are included in three protein complexes: collagen I (COL1), COL6, and laminin 521 (LAM521).

We then tested these protein complexes in DRG *ex vivo* preparations. We found that commercially available human COL6 (H-COL6) could induce orderly axon bundle formation, whereas commercially available rat collagen I (R-COL1) and human-Laminin 521 (H-LAM521) could not (**Figure 3C**). The commercial H-COL6 protein was in the pepsin-resistant triple helical fragment form, and was not contaminated with fibronectin (data not shown).

Moreover, the addition of COL6 (20 μg/mL) to Matrigel (1 mg/mL) promoted axon bundle formation (**Figure 3D** and **E**) and upregulated the expression of NCAM1 at a level comparable to that of the COL6 + Vehicle group, which was approximately three times that in the Matrigel + Vehicle group (**Figure 3F**). The immunofluorescence results also showed an increased axonal NCAM1 fluorescence intensity in the COL6-vehicle and Matrigel-COL6 groups compared with that in the Matrigel-Vehicle group (**Additional Figure 4**). These results pointed at COL6 as the extracellular signal initiating axonal fasciculation, and were consistent with the immunoblot data showing the lack of COL6 in Matrigel components compared to DNM-G components (**Figure 3G**).

We also tested the effects of COL6 on axon bundle formation at lower (4 μg/mL) and higher (100 μg/mL) concentrations in the DRG–Schwann cell co-culture model. The addition of 4 μg/mL COL6 to 1 mg/mL Matrigel resulted in non-compact axon bundles, and the addition of 100 μg/mL COL6 to 1 mg/mL Matrigel caused the detachment of Schwann cells and axons (**Additional Figure 5A** and **B**). Based on our data, the mixture containing 20 μg/mL COL6 + 1 mg/mL Matrigel could induce compact axon bundle formation without affecting the attachment of Schwann cells to axons.

Extracellular COL6 facilitates the distribution of NCAM1 on axolemma

The co-immunoprecipitation-derived protein mass spectrometry data above revealed the interaction between COL6 and NCAM1. Although the co-localization of COL6 and NCAM1 immunofluorescence in the COL6-treated DRG *ex vivo* sample indicated a connection between NCAM1 and COL6 (**Additional Figure 6**), this connection could be direct or indirect, as many other proteins bind them. To exclude any indirect interactions caused by other proteins, we performed immunoprecipitation on a solution containing purified NCAM1 (human isoform NCAM120) and COL6. Using COL6 or NCAM1 as the bait protein, we found that NCAM1 or COL6 could be coimmunoprecipitated and detected by subsequent immunoblotting (**Figure 4A**). The extracellular part of NCAM1 comprises an Ig-like domain and a fibronectin type III-homology domain, and each determines different functions of NCAM1 (Ranheim et al., 1996; Carafoli et al., 2008). Thus, we prepared two recombinant protein segments, one containing five Ig-like domains and the other containing the FN3 domains (**Figure 4B**). According to the co-immunoprecipitation results, when we incubated COL6 with these two protein segments as bait, only the FN3-containing segment could be detected by subsequent immunoblotting (**Figure 4C**).

We next questioned how the binding of NCAM1 with extracellular COL6 can upregulate the expression of NCAM1 in axons, since our real-time polymerase chain reaction showed no increase in the transcription of the *Ncam1* gene in COL6-treated DRGs (**Figure 4D**). Clues from immunofluorescence staining showed two distinct distribution patterns of NCAM1 in neurons: a granular distribution in the cytoplasm (**Figure 4E**) and a smooth distribution on the membrane (**Figure 4E**). The ratio of neurons with smoothly distributed NCAM1 on the membrane was 0.74 ± 0.06 in the COL6 treatment group (M + C), which was higher than that in the vehicle treatment group (M + V, 0.31 ± 0.05, $n = 5$ cultures, $P = 0.0079$, **Figure 4F**). NCAM1 on the cell membrane is reportedly downregulated through endocytosis and the lysosomal degradation pathway (Diestel et al., 2007; Wobst et al., 2012). Therefore, we examined NCAM1 degradation activity via double fluorescence labeling of NCAM1 and lysosomes. Lysosomes-Green Fluorescent Protein vector labeling showed that the ratio of lysosome colocalization with NCAM1 to the total number of lysosomes was significantly reduced in COL6-treated neurons (0.16 ± 0.06) compared to vehicle-treated neurons (0.35 ± 0.09, $n = 20$ cells, $P < 0.0001$, **Figure 4G**).

Collectively, these results suggest that COL6 directly binds to the NCAM1 FN3 domain in extracellular space. This binding inhibits the degradation of membrane NCAM1, thereby leading to increased NCAM1 expression on the cell membrane/axolemma. Previous studies have thoroughly demonstrated that NCAM1 molecules on opposing axolemma regulate the fasciculation of axons through homophilic trans-interactions (Rutishauser et al., 1988; Lin et al., 1994; Cremer et al., 1997; Fujita et al., 2000).

COL6 treatment improves nerve bundle regeneration after sciatic nerve defect

To investigate how COL6-induced axon bundle formation affects peripheral nerve regeneration, we prepared 8-mm

sciatic nerve defects in rats and bridged nerve stumps with silicone catheters filled with 10 mg/mL Matrigel + Vehicle (M + V group) or 10 mg/mL Matrigel + 20 μg/mL COL6 (M + C group). Scanning electron microscopy of the catheter cross sections showed that the addition of 20 μg/mL COL6 to 10 mg/mL Matrigel did not change the porous structure of Matrigel compared with the M + V group (**Additional Figure 7A**).

After 2 weeks of repair, the regenerated axons inside the catheter were immunofluorescence-labeled with an antibody against NF200, and the distribution of COL6 was simultaneously visualized via immunofluorescence labeling. The axons were evenly distributed in the longitudinal sections from the M + C group. For comparison, the axons were mainly distributed at the lateral sides of regenerated nerve tissues in the E and M + V groups. Consistent with the distribution pattern of NF200, COL6 was also evenly distributed in the M + C group, and laterally distributed in the E and M + V groups (**Additional Figure 8A**, upper panel). A fluorescence distribution analysis further confirmed the consistency in the distribution patterns of COL6 and NF200 among all groups (**Additional Figure 8A**, lower panel). Notably, the COL6 signal distribution patterns in the E and M + V groups showed distinct concave curves, suggesting a lack of endogenous COL6 in the regeneration microenvironment, especially at the central area.

After 8 weeks of regeneration, the nerve stumps were well connected with regenerated tissue inside the catheter, and the regenerated tissue in the M + C group had the largest diameter (**Additional Figure 7B** and **C**). Silver staining revealed a certain amount of disorganization among axons in the E and M + V groups. In contrast, in the M + C group, the axons were clustered into bundles that resembled the structure in normal sciatic nerves (**Figure 5A**). Morphological analysis revealed that the width and continuous length of the axon bundles were significantly increased in the M + C group compared with the E and M + V groups ($P < 0.0001$, **Figure 5B** and **C**).

Next, we calculated the axon density in the proximal and distal segments based on fluorescence microscopy of the nerve cross-sections (**Additional Figure 7D** and **E**). In the proximal segment, no significant difference in axon density was detected among the three groups. In contrast, in the distal segment, hydrogel filling (M + V and M + C groups) increased the axon density in both the tibial nerve and peroneal nerve tracts ($P < 0.01$, *vs*. E group, **Additional Figure 7F**). However, no regenerated axons in the central area of the catheters were observed in the M + C group (**Additional Figure 7E**, M + V column, middle row). We divided the regions containing the tibial nerve tract and peroneal nerve tract into four quadrants (**Additional Figure 7G**). The uniformity of axon distribution in the nerve tract could be quantitatively reflected by the coefficient of variation of axon density between the different quadrants. We found a high coefficient of variation in the M + V group, whereas the addition of COL6 to the Matrigel decreased this value to a normal level ($P < 0.0001$, **Additional Figure 7H**).

Moreover, we analyzed the accuracy of nerve bundle projections via retrograde fluorescence tracing of the tibial nerve tract (**Figure 5D** and **Additional Figure 8B**). After 5 days of tracing, the accuracy of the tibial nerve projection in the M + V group was lower than that in the M + C group (**Figure 5E**, 0.72 ± 0.02 *vs.* 0.81 ± 0.04, $n = 5$, $P = 0.0014$).

Functionally, after 8 weeks of repair, the empty silica catheter bridging (E) only resulted in a 6.42 ± 1.78% increase in sciatic nerve CMAP. Filling the silicone catheter with 10 mg/mL Matrigel (M + V) enhanced the recovery of CMAP to 27.46 ± 4.22%, and the addition of 20 μg/mL COL6 to Matrigel (M + C) further increased the recovery of CMAP to 43.05 ± 6.75%. The motor nerve conduction velocities were not significantly different between the M + V and M + C groups (**Figure 5F**). The sciatic nerve function index data also showed the highest functional recovery level in the M + C treatment group (–60.91 ± 9.89), compared with that in the M + V (–68.82 ± 5.78) and E (–78.66 ± 5.15, $n = 5$, **Figure 5G**) groups.

Taken together, the results of this study revealed that the binding of extracellular COL6 to the NCAM1 FN3 domain prevents the lysosomal degradation of NCAM1, resulting in the accumulation of NCAM1 on the axolemma. Subsequently, the NCAM1 molecules on the axolemma promote axonal fasciculation that facilitates the formation of nerve bundle structure (**Figure 6**).

Discussion

Our data support the important role of the ECM microenvironment in the regeneration of nerve bundle structure. The fasciculation of axons in DNM-G but not in Matrigel, laminin, COL1, or COL4 suggests a tissue-specific function of the peripheral nerve microenvironment in promoting the formation of axon bundles. Although we found the lack of axonal NCAM1 to be the cause of axonal disorganization, the overexpression of NCAM1 in neurons could not rescue the dispersed axons in Matrigel. Instead, the overexpressed NCAM1 molecules had mostly accumulated in the DRG soma and were not distributed on the axolemma. These results indicate that the distribution of NCAM1 on the axolemma relies on some environmental cues that are unique to DNM-G or the peripheral nerve ECM.

Next, we identified COL6 as the environmental cue that immobilizes NCAM1 on the cell membrane/axolemma. Thus, COL6-NCAM1 is a cooperative unit that controls axon bundle formation, in which COL6 acts as the extracellular signal initiating axonal fasciculation. In most cases, patients with a peripheral nerve injury do not have a NCAM1 deficiency. Therefore, this finding highlights the role of COL6 in nerve bundle regeneration.

Peltonen et al. (1990) and Braghetta et al. (1996) reported that COL6 is abundantly expressed by Schwann cells. Thus, endogenous Schwann cells might promote axon bundle formation after injury. Indeed, we found low expression of endogenous COL6 in the regenerated nerve tissue. However, the disorganized axon regeneration suggests that the content of endogenous COL6 is not sufficient to support nerve bundle formation across an 8-mm gap in rats. Therefore, it was necessary to artificially increase the content of COL6 in the microenvironment, which can be easily realized by hydrogel filling or solution permeation.

Moreover, our *in vitro* experiments showed that during axonal fasciculation in the COL6 + Vehicle (C + V) group, the migration distance of Schwann cells lagged far behind the growth distance of axon bundles (**Additional Video 1**). Furthermore, most Schwann cells detached from axons after COL6 treatment (**Additional Video 1** and **Additional Figure 5**). These results indicate that COL6-induced axonal bundle formation occurs independently of Schwann cells. Additionally, the detachment of Schwann cells and axons in response to a high concentration of COL6 indicates that COL6 has an inhibitory effect on myelination. This finding is consistent with a previous report showing that the lack of COL6 in Col6a1$^{-/-}$ mice leads to the hypermyelination of axons in the peripheral nervous system (Chen et al., 2015). Taken together, these results point to a dual myelination function of COL6, which occurs in a dose-dependent manner.

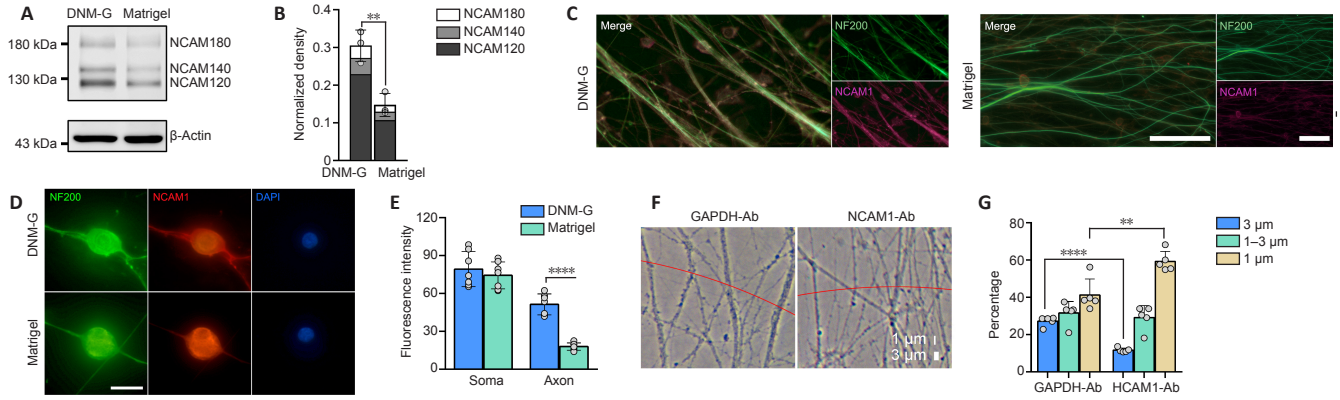

Figure 2 | **NCAM1 mediates the clustering of neurites.**
(A, B) Immunoblotting confirming the upregulation of all three NCAM1 isoforms (NCAM120, NCAM140, and NCAM180) in DNM-G-treated DRGs, compared with Matrigel-treated DRGs (n = 3 independent experiments, $^{**}P$ = 0.0063, Student's t-test). The expression of NCAM1 was normalized to β-actin. (C) Immunofluorescence images of NCAM1 (red, stained by Cy3) expression in axons (labeled with NF200, green, stained by Alexa Fluor 488). The NCAM1 signals in the DNM-G group were stronger than those in the Matrigel group. (D) Immunofluorescence images showing the lack of NCAM1 (red, stained by Cy3) in axons but not somas in the Matrigel group, compared with the DNM-G group. (E) Comparison of NCAM1 fluorescence intensity in DRG somas and axons between the DNM-G and Matrigel groups (n = 7 cultures, $^{****}P < 0.0001$, Student's t-test). (F) Phase contrast microscopy of single axons/axon bundles in DNM-G after antibody blocking for 48 hours. The red line indicates a 1-mm distance from the DRG tissue block center. We measured the diameter of each axon or bundle across the red line. (G) Distributions of axon bundle diameters after GAPDH-Ab and NCAM1-Ab treatments (n = 5 cultures, $^{**}P < 0.01$, $^{****}P < 0.0001$, Student's t-test). Scale bars: 50 μm in C and 8 μm in D. DNM-G: Decellularized nerve matrix-gel; DRG: dorsal root ganglion; GAPDH: glyceraldehyde-3-phosphate dehydrogenase; NCAM1: neural cell adhesion molecule 1.

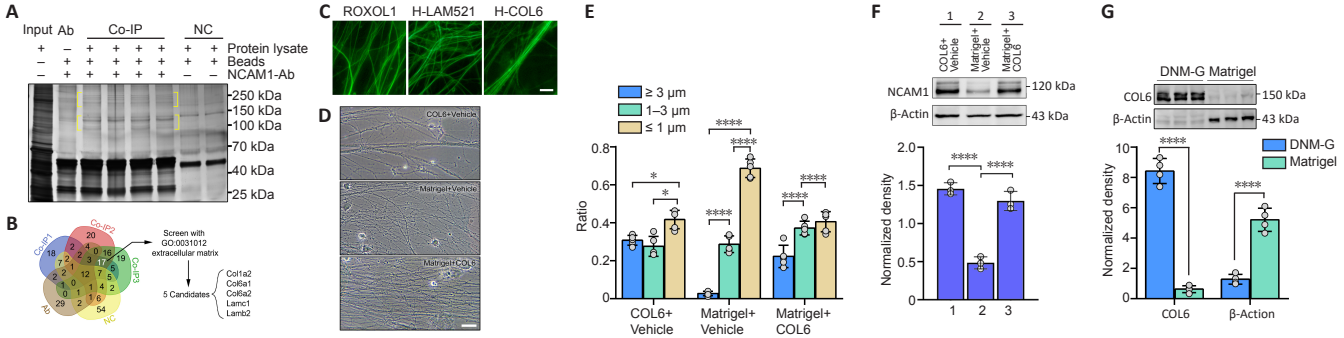

Figure 3 | **Identification of COL6 as the extracellular signal initiating axonal fasciculation.**
(A) Total protein bands in the different groups. Protein bands were detected using Tris-Glycine eXtended Stain-Free technology. Yellow brackets indicate the specific protein bands in the co-immunoprecipitation group. (B) Set analysis of liquid chromatography-mass spectrometry/mass spectrometry results identified 17 protein candidates, and subsequent GO annotation further identified 5 ECM candidates out of 17. (C) Representative images of axons growing on substrates of rat collagen 1 (R-COL1), human laminin 521 (H-LAM521), and human collagen 6 (H-COL6). Distinct axonal fasciculation occured only in the H-COL6 group. (D) Representative images showing axonal trajectories in different groups. Axonal fasciculations were observed in the COL6-rich substrates (COL6 + Vehicle and Matrigel + COL6 groups) but not in the Matrigel + Vehicle substrate. (E) Axon bundle diameter distribution (n = 5 cultures, $^{*}P < 0.05$, $^{****}P < 0.0001$, one-way analysis of variance followed by Tukey's multiple comparison tests). (F) Immunoblotting of NCAM1 in DRGs *ex vivo* preparations growing on different substrates. Histogram of densitometry showing increased NCAM1 levels in the COL6 + vehicle (1) and Matrigel + COL6 (3) groups, compared with that in the Matrigel + vehicle (2) group (n = 3 cultures, $^{****}P < 0.0001$, Kruskal-Wallis test followed by Dunn-Bonferroni *post hoc* test). (G) Immunoblotting of COL6 and β-actin in the components of DNM-G and Matrigel. The histogram of densitometry shows a lower COL6 level and a higher β-actin level in Matrigel, compared with that in DNM-G (normalized by total protein, n = 4 independent experiments, $^{****}P < 0.0001$, Student's t-test). Scale bars: 5 μm in C and 20 μm in D. COL6: Collagen VI; DNM-G: decellularized nerve matrix-gel; GO: gene ontology; H-COL6: human collagen 6; H-LAM521: human laminin 521; R-COL1: rat collagen 1.

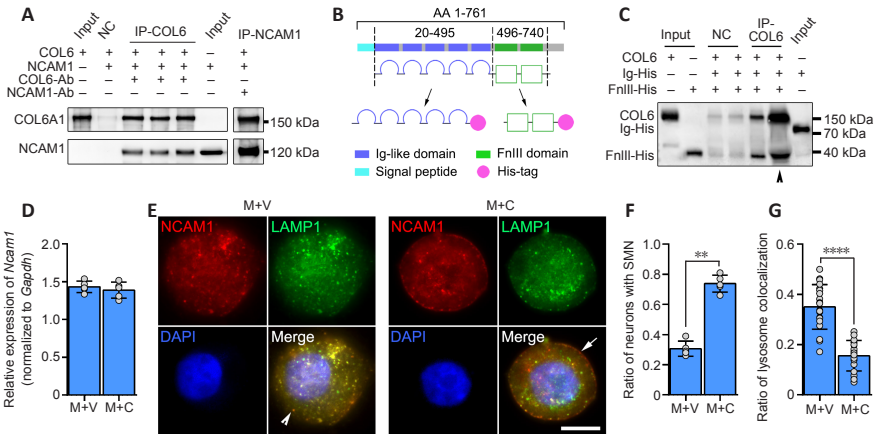

Figure 4 | **COL6-NCAM1 interaction inhibits lysosomal degradation of NCAM1.**
(A) Co-immunoprecipitation revealed a direct interaction between COL6 and NCAM1 (isoform NCAM120). (B) Schematic diagram of recombinant protein domain construction. (C) Co-immunoprecipitation demonstrated that COL6 interacted with the NCAM1 FN3 domain but not the Ig-like domain. Arrowheads indicate five times the amount of proteins for the same assay. (D) qRT-PCR analyses of *Ncam1* genes in DRGs growing on M + V and M + C substrates. *Gapdh* was used as the reference gene (n = 5 cultures, P = 0.4704, Student's t-test). (E) Representative fluorescence images of NCAM1 (red, stained by Cy3) and lysosomes (green, stained by lysosomes-GFP) in DRG somas. In the M + V group, the lysosomes were predominantly scattered in the cytoplasm (arrowhead indicates granular cytoplasmic NCAM1). In the M + C group, the lysosomes were mainly distributed on the membrane (arrow indicates smooth membrane NCAM1). (F) The ratio of neurons with SMN, compared between groups (n = 5 cultures, $^{**}P$ = 0.0079, Wilcoxon-Mann-Whitney test). (G) The ratio of lysosome colocalization with NCAM1, manually counted, revealed a significant reduction in COL6-treated (M + C) DRGs compared with vehicle-treated (M + V) DRGs (n = 20 cells from three independent experiments, $^{****}P < 0.0001$, Student's t-test). Scale bar: 5 μm in E. COL6: Collagen VI; DRG: dorsal root ganglion; FN3: fibronectin type III domains; Gapdh: glyceraldehyde-3-phosphate dehydrogenase; GFP: green fluorescent protein; M + V: Matrigel + Vehicle; M + C: Matrigel + COL6; NCAM1: neural cell adhesion molecule 1; qRT-PCR: real-time quantitative reverse transcription-polymerase chain reaction; SMN: smooth membrane NCAM1.

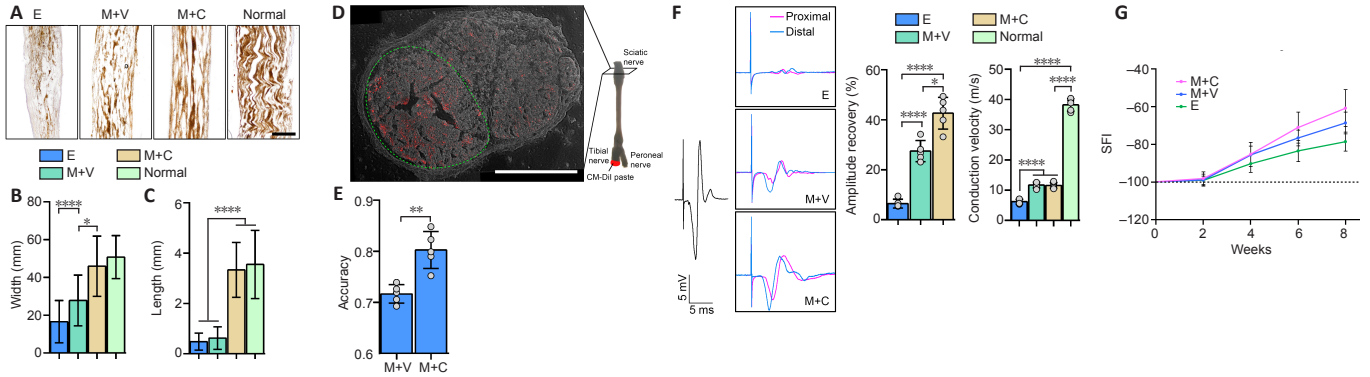

Figure 5 | **Addition of COL6 in Matrigel improves structural and functional recovery of sciatic nerve defect.**
(A) Longitudinal sections with silver staining show regenerated nerves in catheters. The M + C group had the most orderly nerve bundles. (B) Widths of axon bundles, measured and compared among different groups (n = 16 slices from five animals, *P = 0.0360, ****P < 0.0001, one-way analysis of variance followed by Tukey's multiple comparison tests). (C) The continuous lengths of the axon bundles, measured and compared among different groups (n = 16 slices from five animals, ****P < 0.0001, one-way analysis of variance followed by Tukey's multiple comparison tests). (D) A sciatic nerve cross-section shows the retrograde fluorescence tracing on the tibial nerve tract in the M + C group. The green dotted line marks the region of the tibial nerve tract, and the red dots indicate the fluorescence positive axons. (E) Accuracy of tibial nerve projection in the M + C and M + V groups (n = 5 animals, **P = 0.0014, Student's t-test). (F) After 8 weeks of regeneration, we measured the CMAP in the sciatic nerve in different groups. Panels show representative traces of CMAP in the E, M + V, and M + C groups. The amplitude of CMAP in the M + C group was larger than those in the other groups. The black trace on the left indicates CMAP recorded from a normal sciatic nerve. The histogram on the upper right shows the amplitude recovery of the injured sciatic nerve (n = 5 animals, ***P = 0.0005, ****P < 0.0001, one-way analysis of variance followed by Tukey's multiple comparison tests). The histogram on the lower right shows the motor nerve conduction velocity between the groups (n = 5 animals, ****P < 0.0001, one-way analysis of variance followed by Tukey's multiple comparison tests). (G) SFI of rats at different time points. Scale bars: 400 μm in A and D. CMAP: Compound muscle action potential; COL6: collagen VI; E: empty; M + C: Matrigel + COL6; M + V: Matrigel + Vehicle; SFI; sciatic nerve function index.

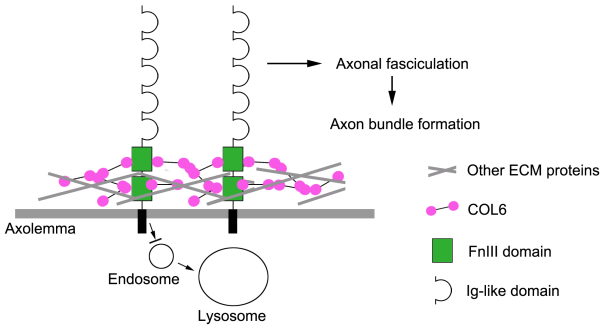

Figure 6 | **Mechanisms of COL6-initiated nerve bundle formation.**
Illustration of our hypothetical mechanism underlying axon bundle formation during peripheral nerve regeneration. COL6: Collagen VI; ECM: extracellular matrix; FnIII: fibronectin type III domains.

Our protein interaction assay demonstrated the direct binding of NCAM1 and COL6. Although we only tested NCAM120 in these experiments, considering that the three major NCAM1 isoforms (NCAM120, NCAM140, and NCAM180) share identical extracellular domains, it is reasonable to speculate that COL6 exerts the same effects on all three protein isoforms. The binding of NCAM1 to extracellular COL6 immobilizes NCAM1 on the cell membrane. In a previous study, researchers demonstrated that a COL6 deficiency caused fragmentation of acetylcholine receptor clusters (Cescon et al., 2018), resembling the destruction of NCAM1 integrity on the cell membrane when DRG neurons were cultured in a COL6-free environment. These results indicate that the COL6-dependant immobilization of proteins on the cytomembrane may be a common pathogenic mechanism underlying COL6 deficiency-related diseases. More importantly, our study is the first to report the binding of COL6 to the NCAM1 FN3 domain. The FN3 domain is an evolutionarily conserved protein domain that is widely found in animal proteins. It is a common interaction site shared by multiple biological processes, including cell adhesion, migration proliferation, muscle tissue development, and tumorigenesis (Bencharit et al., 2007; Henderson et al., 2017; Wuensch et al., 2019). Accordingly, COL6 may also influence these biological processes.

Many studies have shown that gradient-distributed biochemical cues (Tang et al., 2013) or well-aligned physical structures (Mobasseri et al., 2015) can effectively reduce disordered nerve regeneration by guiding the direction of growing axons. The present findings suggest that COL6-initiated axonal fasciculation can further increase the directional stability of regenerating axons by unifying the directions of different axons as axon bundles, thus enhancing orderly nerve regeneration. Based on this finding, we propose that COL6 is important for orderly nerve bundle regeneration following severe peripheral nerve damage (e.g., nerve defect).

For minor nerve damage cases (e.g., nerve crush), the preserved endoneurial tubes provide correct routes for nerve regeneration, and the endoneurial sheath separates growing axons. Hence, COL6-NCAM1-mediated axonal fasciculation may not be necessary in these cases. However, other studies have nerve bundles and improved functional recovery following COL6 treatment. Our nerve tracing results suggest that the improved nerve function in the M + C group could mainly be attributed to the increased projection accuracy of regenerative axons, as we found no significant differences in nerve conduction velocity or the quantity of regenerated axons between the M + V and M + C groups. Given that parallel nerve bundles/tracts are abundant in the white matter of the spinal cord, COL6 administration may be a suitable strategy for improving the accuracy of spinal cord regeneration.

As a shortcoming, we found that COL6-induced axonal fasciculation improved only the orderliness of the nerve bundle structure but not the goal-oriented pathfinding of regenerating axons. Therefore, in practice, it may be necessary to use COL6 in combination with guidance cues and/or other regeneration promoting factors that play reciprocal roles.

In this study, we putatively selected NCAM1 as the downstream signal of axonal fasciculation and traced backwards to its upstream signal, which was demonstrated to be COL6. Although our data demonstrate that both COL6 and NCAM1 play a role in nerve bundle formation, our research design was limited in that we could not exclude other

compounds that directly interact with COL6 (e.g., fibronectin COL1, COL2, matrilin-1, fibulin-2, and hyaluronan). Thus, these may also contribute to the observed effects. Future systemic studies involving high-throughput proteome analysis and knockdown models could further reveal the complete signaling pathways underlying nerve bundle formation.

In conclusion, we identified COL6 as an important extracellular signal for axonal fasciculation and revealed the interaction between COL6 and NCAM1 in regulating nerve bundle formation. These findings not only expand upon our understanding of how the ECM environment affects the organization of regenerating axons, but also provide the foundation for a promising therapeutic strategy to reduce axonal disorganization during nerve regeneration.

Acknowledgments: *We gratefully acknowledge the Guangzhou Medical University Large-Scale Experimental Apparatus Sharing Platform for their technical support.*
Author contributions: *Study design: JLZ, JHS, DPQ, YMW, YY; experiment implementation: JHS, MH, ZF, TTW, YC, YYX, JLZ; data analysis: TXL, JLZ, MH; manuscript writing: JLZ, JHS, YY. All authors read and approved the final version of the manuscript.*
Conflicts of interest: *The authors declare no conflict of interest.*
Financial support: *This study was supported by the National Natural Science Foundation of China, No. 31800892 (to JLZ); the Natural Science Foundation of Guangdong Province of China, No. 2018A030310254 (to YY); and a grant from Guangzhou Medical University Start-up Project of China, No. B195002002048 (to JLZ). The funding sources had no role in study conception and design, data analysis or interpretation, paper writing or deciding to submit this paper for publication.*
Institutional review board statement: *This study was approved by the Animal Ethics Committee of Guangzhou Medical University (approval No. GY2019048) on April 30, 2019.*
Copyright license agreement: *The Copyright License Agreement has been signed by all authors before publication.*
Data sharing statement: *Datasets analyzed during the current study are available from the corresponding author on reasonable request.*
Plagiarism check: *Checked twice by iThenticate.*
Peer review: *Externally peer reviewed.*
Open access statement: *This is an open access journal, and articles are distributed under the terms of the Creative Commons Attribution-NonCommercial-ShareAlike 4.0 License, which allows others to remix, tweak, and build upon the work non-commercially, as long as appropriate credit is given and the new creations are licensed under the identical terms.*

Additional files:

Additional Figure 1: *Morphology of axons growing on laminin 521 (bright field microscopy), COL1 and COL4 (immunofluorescence microscopy) substrates.*
Additional Figure 2: *Measurement of axons/axon bundle diameters.*
Additional Figure 3: *DNM-G upregulates expression level of NCAM1 in axons.*
Additional Figure 4: *Fluorescence microscopy of NCAM1 (red, stained by Cy3) and NF200 (green, stained by Alexa Fluor 488) in different groups.*
Additional Figure 5: *High concentration of COL6 inhibits the attachment of Schwann cells to axons.*
Additional Figure 6: *Colocalization of COL6 and NCAM1.*
Additional Figure 7: *COL6 improves the uniformity of regenerated axon distribution in the distal nerve trunk.*
Additional Figure 8: *Distribution patterns of NF200 and COL6 in the regenerated nerve tissues.*
Additional Video 1: *Dynamics of axon bundle formation in different ECM environment.*

References

Bencharit S, Cui CB, Siddiqui A, Howard-Williams EL, Sondek J, Zuobi-Hasona K, Aukhil I (2007) Structural insights into fibronectin type III domain-mediated signaling. J Mol Biol 367:303-309.

Braghetta P, Fabbro C, Piccolo S, Marvulli D, Bonaldo P, Volpin D, Bressan GM (1996) Distinct regions control transcriptional activation of the alpha1(VI) collagen promoter in different tissues of transgenic mice. J Cell Biol 135:1163-1177.

Carafoli F, Saffell JL, Hohenester E (2008) Structure of the tandem fibronectin type 3 domains of neural cell adhesion molecule. J Mol Biol 377:524-534.

Cattin AL, Lloyd AC (2016) The multicellular complexity of peripheral nerve regeneration. Curr Opin Neurobiol 39:38-46.

Cescon M, Chen P, Castagnaro S, Gregorio I, Bonaldo P (2016) Lack of collagen VI promotes neurodegeneration by impairing autophagy and inducing apoptosis during aging. Aging (Albany NY) 8:1083-1101.

Cescon M, Gregorio I, Eiber N, Borgia D, Fusto A, Sabatelli P, Scorzeto M, Megighian A, Pegoraro E, Hashemolhosseini S, Bonaldo P (2018) Collagen VI is required for the structural and functional integrity of the neuromuscular junction. Acta Neuropathol 136:483-499.

Chen CH, Hsu HW, Chang YH, Pan CL (2019) Adhesive L1CAM-Robo signaling aligns growth cone f-actin dynamics to promote axon-dendrite fasciculation in C. elegans. Dev Cell 48:215-228.e5.

Chen P, Cescon M, Megighian A, Bonaldo P (2014) Collagen VI regulates peripheral nerve myelination and function. FASEB J 28:1145-1156.

Chen P, Cescon M, Zuccolotto G, Nobbio L, Colombelli C, Filaferro M, Vitale G, Feltri ML, Bonaldo P (2015) Collagen VI regulates peripheral nerve regeneration by modulating macrophage recruitment and polarization. Acta Neuropathol 129:97-113.

Chooi WH, Chew SY (2019) Modulation of cell-cell interactions for neural tissue engineering: Potential therapeutic applications of cell adhesion molecules in nerve regeneration. Biomaterials 197:327-344.

Chu C, Gao Y, Lan X, Thomas A, Li S (2018) NCAM mimetic peptides: potential therapeutic target for neurological disorders. Neurochem Res 43:1714-1722.

Cremer H, Chazal G, Goridis C, Represa A (1997) NCAM is essential for axonal growth and fasciculation in the hippocampus. Mol Cell Neurosci 8:323-335.

Crossin KL, Krushel LA (2000) Cellular signaling by neural cell adhesion molecules of the immunoglobulin superfamily. Dev Dyn 218:260-279.

Cunningham BA, Hemperly JJ, Murray BA, Prediger EA, Brackenbury R, Edelman GM (1987) Neural cell adhesion molecule: structure, immunoglobulin-like domains, cell surface modulation, and alternative RNA splicing. Science 236:799-806.

de Luca AC, Lacour SP, Raffoul W, di Summa PG (2014) Extracellular matrix components in peripheral nerve repair: how to affect neural cellular response and nerve regeneration? Neural Regen Res 9:1943-1948.

de Ruiter GC, Spinner RJ, Verhaagen J, Malessy MJ (2014) Misdirection and guidance of regenerating axons after experimental nerve injury and repair. J Neurosurg 120:493-501.

Diestel S, Schaefer D, Cremer H, Schmitz B (2007) NCAM is ubiquitylated, endocytosed and recycled in neurons. J Cell Sci 120:4035-4049.

Eggers K, Werneburg S, Schertzinger A, Abeln M, Schiff M, Scharenberg MA, Burkhardt H, Mühlenhoff M, Hildebrandt H (2011) Polysialic acid controls NCAM signals at cell-cell contacts to regulate focal adhesion independent from FGF receptor activity. J Cell Sci 124:3279-3291.

Elazar N, Vainshtein A, Golan N, Vijayaragavan B, Schaeren-Wiemers N, Eshed-Eisenbach Y, Peles E (2019) Axoglial adhesion by Cadm4 regulates CNS myelination. Neuron 101:224-231.e5.

English AW (2005) Enhancing axon regeneration in peripheral nerves also increases functionally inappropriate reinnervation of targets. J Comp Neurol 490:427-441.

Ferrer-Ferrer M, Dityatev A (2018) Shaping synapses by the neural extracellular matrix. Front Neuroanat 12:40.

Fujita N, Saito R, Watanabe K, Nagata S (2000) An essential role of the neuronal cell adhesion molecule contactin in development of the Xenopus primary sensory system. Dev Biol 221:308-320.

Giger RJ, Hollis ER, 2nd, Tuszynski MH (2010) Guidance molecules in axon regeneration. Cold Spring Harb Perspect Biol 2:a001867.

Gonzalez-Perez F, Udina E, Navarro X (2013) Extracellular matrix components in peripheral nerve regeneration. Int Rev Neurobiol 108:257-275.

Groulx JF, Gagné D, Benoit YD, Martel D, Basora N, Beaulieu JF (2011) Collagen VI is a basement membrane component that regulates epithelial cell-fibronectin interactions. Matrix Biol 30:195-206.

He XZ, Wang W, Hu TM, Ma JJ, Yu CY, Gao YF, Cheng XL, Wang P (2016) Peripheral nerve repair: theory and technology application. Zhongguo Zuzhi Gongcheng Yanjiu 20:1044-1050.

Henderson CA, Gomez CG, Novak SM, Mi-Mi L, Gregorio CC (2017) Overview of the muscle cytoskeleton. Compr Physiol 7:891-944.

Kolkova K, Novitskaya V, Pedersen N, Berezin V, Bock E (2000) Neural cell adhesion molecule-stimulated neurite outgrowth depends on activation of protein kinase C and the Ras-mitogen-activated protein kinase pathway. J Neurosci 20:2238-2246.

Li S, Leshchyns'ka I, Chernyshova Y, Schachner M, Sytnyk V (2013) The neural cell adhesion molecule (NCAM) associates with and signals through p21-activated kinase 1 (Pak1). J Neurosci 33:790-803.

Lin DM, Fetter RD, Kopczynski C, Grenningloh G, Goodman CS (1994) Genetic analysis of Fasciclin II in Drosophila: defasciculation, refasciculation, and altered fasciculation. Neuron 13:1055-1069.

Mathot F, Rbia N, Thaler R, Dietz AB, van Wijnen AJ, Bishop AT, Shin AY (2021) Gene expression profiles of human adipose-derived mesenchymal stem cells dynamically seeded on clinically available processed nerve allografts and collagen nerve guides. Neural Regen Res 16:1613-1621.

Mobasseri A, Faroni A, Minogue BM, Downes S, Terenghi G, Reid AJ (2015) Polymer scaffolds with preferential parallel grooves enhance nerve regeneration. Tissue Eng Part A 21:1152-1162.

Neiiendam JL, Køhler LB, Christensen C, Li S, Pedersen MV, Ditlevsen DK, Kornum MK, Kiselyov VV, Berezin V, Bock E (2004) An NCAM-derived FGF-receptor agonist, the FGL-peptide, induces neurite outgrowth and neuronal survival in primary rat neurons. J Neurochem 91:920-935.

Nielsen J, Kulahin N, Walmod PS (2010) Extracellular protein interactions mediated by the neural cell adhesion molecule, NCAM: heterophilic interactions between NCAM and cell adhesion molecules, extracellular matrix proteins, and viruses. Adv Exp Med Biol 663:23-53.

Peltonen J, Jaakkola S, Hsiao LL, Timpl R, Chu ML, Uitto J (1990) Type VI collagen. In situ hybridizations and immunohistochemistry reveal abundant mRNA and protein levels in human neurofibroma, schwannoma and normal peripheral nerve tissues. Lab Invest 62:487-492.

Ranheim TS, Edelman GM, Cunningham BA (1996) Homophilic adhesion mediated by the neural cell adhesion molecule involves multiple immunoglobulin domains. Proc Natl Acad Sci U S A 93:4071-4075.

Raza C, Riaz HA, Anjum R, Shakeel NUA (2020) Repair strategies for injured peripheral nerve: Review. Life Sci 243:117308.

Rutishauser U, Acheson A, Hall AK, Mann DM, Sunshine J (1988) The neural cell adhesion molecule (NCAM) as a regulator of cell-cell interactions. Science 240:53-57.

Sun JH, Li G, Wu TT, Lin ZJ, Zou JL, Huang LJ, Xu HY, Wang JH, Ma YH, Zeng YS (2020) Decellularization optimizes the inhibitory microenvironment of the optic nerve to support neurite growth. Biomaterials 258:120289.

Tang S, Zhu J, Xu Y, Xiang AP, Jiang MH, Quan D (2013) The effects of gradients of nerve growth factor immobilized PCLA scaffolds on neurite outgrowth in vitro and peripheral nerve regeneration in rats. Biomaterials 34:7086-7096.

Urciuolo A, Quarta M, Morbidoni V, Gattazzo F, Molon S, Grumati P, Montemurro F, Tedesco FS, Blaauw B, Cossu G, Vozzi G, Rando TA, Bonaldo P (2013) Collagen VI regulates satellite cell self-renewal and muscle regeneration. Nat Commun 4:1964.

Van Vactor D (1998) Adhesion and signaling in axonal fasciculation. Curr Opin Neurobiol 8:80-86.

Wagner R, DeLeo JA, Coombs DW, Myers RR (1995) Gender differences in autotomy following sciatic cryoneurolysis in the rat. Physiol Behav 58:37-41.

Wobst H, Förster S, Laurini C, Sekulla A, Dreiseidler M, Höhfeld J, Schmitz B, Diestel S (2012) UCHL1 regulates ubiquitination and recycling of the neural cell adhesion molecule NCAM. FEBS J 279:4398-4409.

Wuensch T, Wizenty J, Quint J, Spitz W, Bosma M, Becker O, Adler A, Veltzke-Schlieker W, Stockmann M, Weiss S, Biebl M, Pratschke J, Aigner F (2019) Expression analysis of fibronectin type III domain-containing (FNDC) genes in inflammatory bowel disease and colorectal cancer. Gastroenterol Res Pract 2019:3784172.

You WK, Bonaldo P, Stallcup WB (2012) Collagen VI ablation retards brain tumor progression due to deficits in assembly of the vascular basal lamina. Am J Pathol 180:1145-1158.

Yuan YS, Yu F, Zhang YJ, Niu SP, Xu HL, Kou YH (2021) Changes in proteins related to early nerve repair in a rat model of sciatic nerve injury. Neural Regen Res 16:1622-1627.

Zou JL, Liu S, Sun JH, Yang WH, Xu YW, Rao ZL, Jiang B, Zhu QT, Liu XL, Wu JL, Chang C, Mao HQ, Ling EA, Quan DP, Zeng YS (2018) Peripheral nerve-derived matrix hydrogel promotes remyelination and inhibits synapse formation. Adv Funct Mater 28:1705739.

C-Editor: Zhao M; S-Editors: Yu J, Li CH; L-Editors: Yu J, Song LP; T-Editor: Jia Y

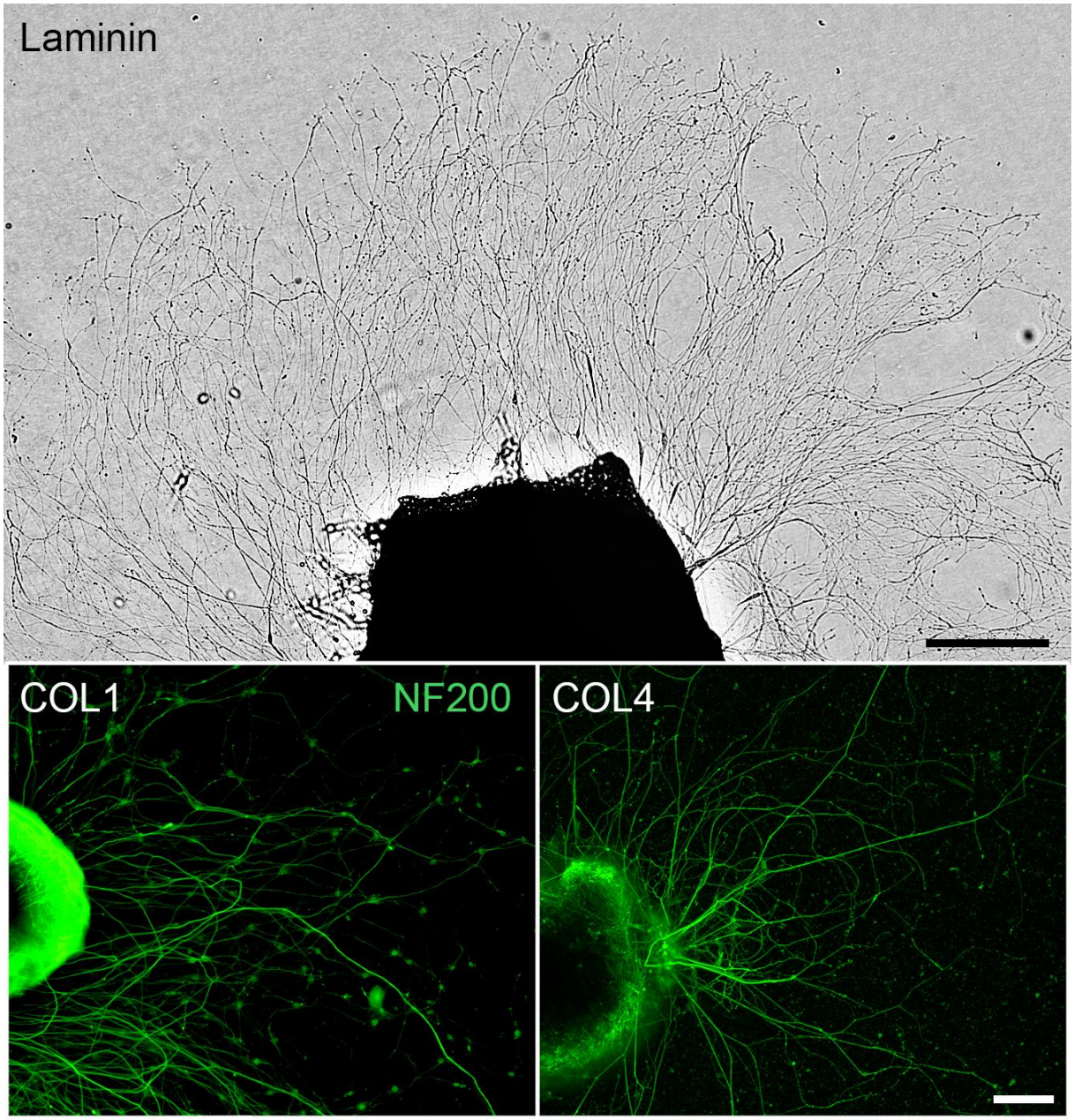

Additional Figure 1 Morphology of axons growing on laminin 521 (bright field microscopy), COL1 and COL4 (immunofluorescence microscopy) substrates.

Axons are marked with NF200 (green, stained by Alexa Fluor 488). Scale bars: 300 μm. COL1: Collagen I; COL4: collagen IV; NF200: Neurofilament 200. These representative images come from three repetitions of experiment.

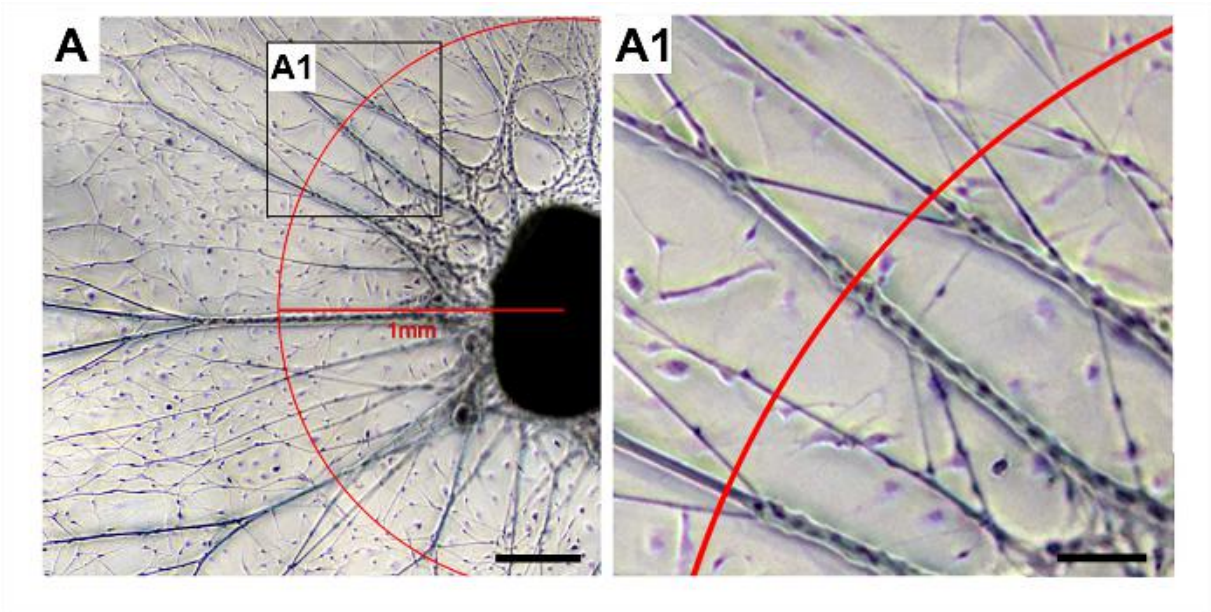

Additional Figure 2 Measurement of axons/axon bundle diameters.

(A) Representative picture of DRG tissue block growing on DNM-G, the red circle indicates 1 mm distance to DRG tissue block center. (A1) We measured the diameter of each axon/axon bundle across the red line in the enlarged view. Scale bar: 300 μm (A) 100 μm (A1). DNM-G: Decellularized nerve matrix-gel; DRG: dorsal root ganglion. Three repetitions of the experiment are performed.

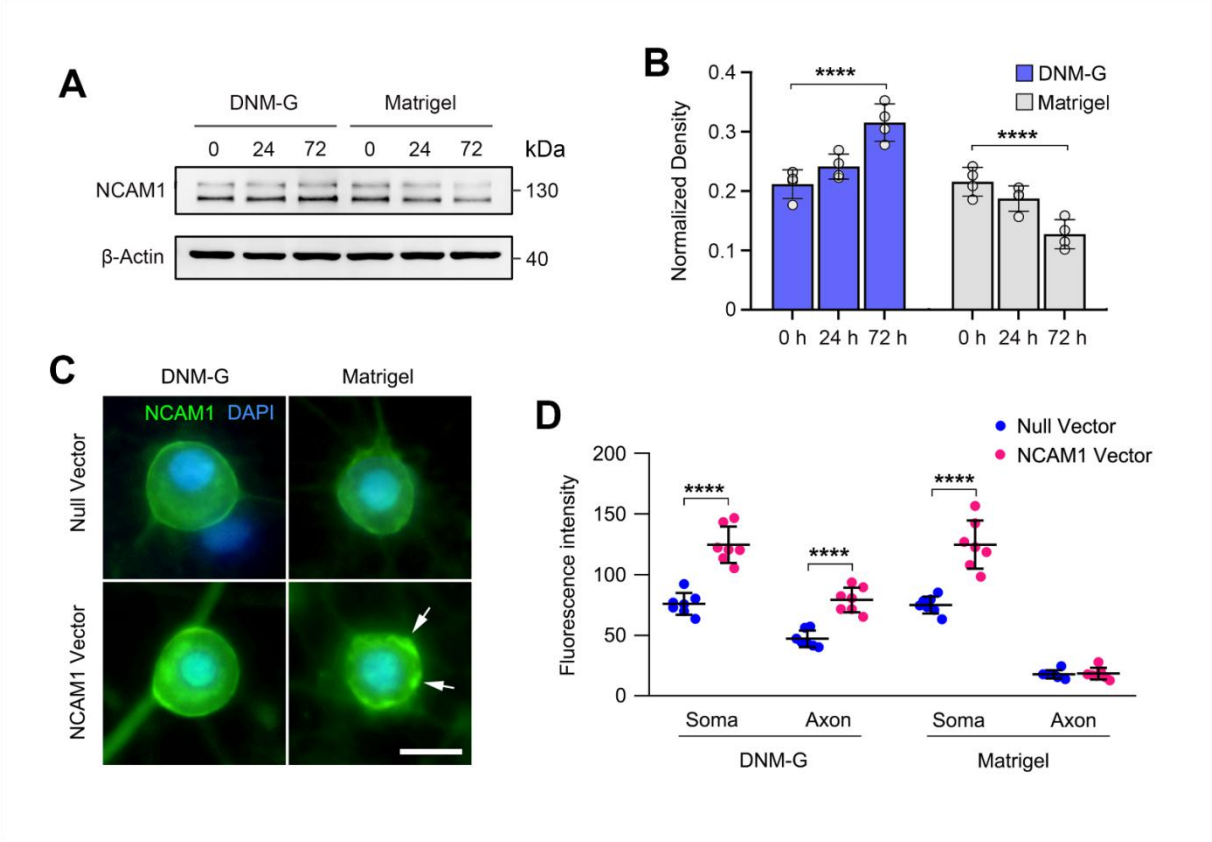

Additional Figure 3 DNM-G upregulates expression level of NCAM1 in axons.

(A) NCAM1 in DNM-G- and Matrigel-treated DRGs were quantified by immunoblotting at different timepoints. (B) Dynamic change of NCAM1 level with the development of time in DNM-G- and Matrigel-treated DGRs (n = 4 experiments, ****$P < 0.0001$, one-way analysis of variance followed by Tukey's multiple comparison tests). (C) Fluorescence microscopy showed NCAM1 (green, stained by Alexa Fluor 488) in DRG neurons after plasmid transfection. Arrows indicate accumulated NCAM1 in DRG soma. (D) In DNM-G the overexpression of NCAM1 increased the fluorescence intensity of NCAM1 in both DRG somas and axons, but in Matrigel the fluorescence intensity of NCAM1 only increased in DRG somas (n = 7 cultures, ****$P < 0.0001$, Student's t-test). Scale bar: 10 μm (C). DNM-G: Decellularized nerve matrix-gel; DRG: dorsal root ganglion; NCAM1: neural cell adhesion molecule 1.

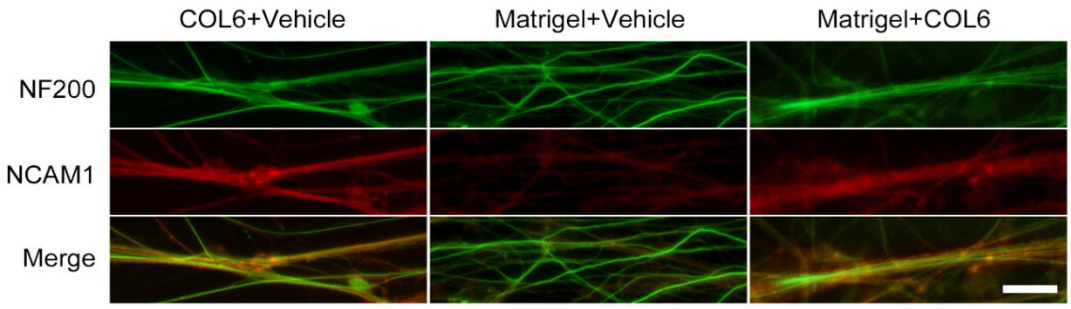

Additional Figure 4 Fluorescence microscopy of NCAM1 (red, stained by Cy3) and NF200 (green, stained by Alexa Fluor 488) in different groups.

This experiment has been repeated three times. Scale bar: 20 μm. NCAM1: Neural cell adhesion molecule 1; NF200: neurofilament 200.

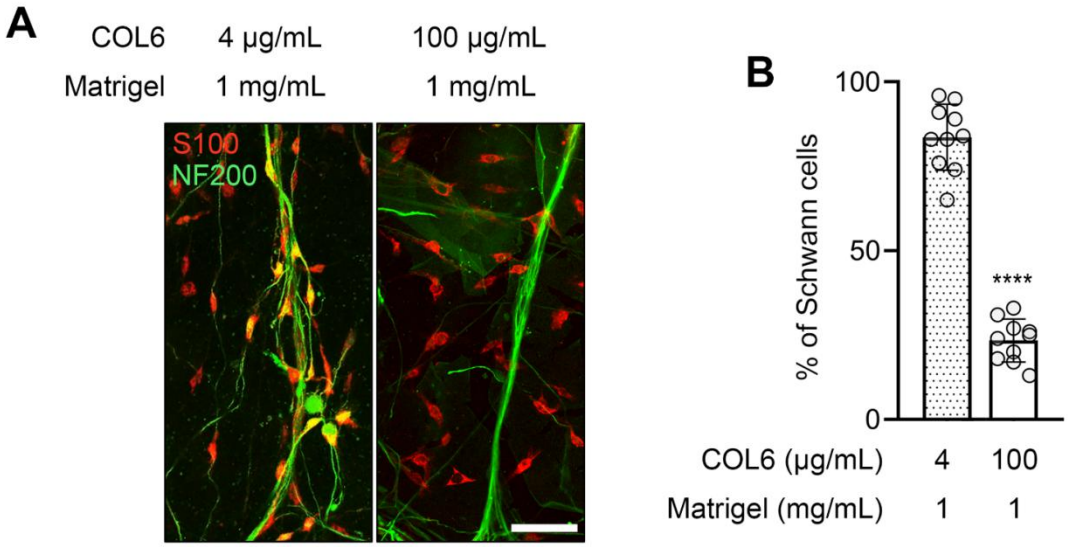

Additional Figure 5 High concentration of COL6 inhibits the attachment of Schwann cells to axons.

After 3 days of DRG–Schwann cells coculturing, the Schwann cells are labeled with antibody against S100, and the axons are labeled with antibody against NF200. (A) Fluorescent confocal microscopy showing the interaction of Schwann cells (marked with S100, red, stained by Cy3) and axons (marked with NF200, green, stained by Alexa Fluor 488) in different groups. (B) The percentage of Schwann cells attached to axons is compared between the two groups (n = 10 cultures, ****$P < 0.0001$, Student's *t*-test). Scale bar: 60 μm (A). COL6: Collagen VI; NF200: neurofilament 200.

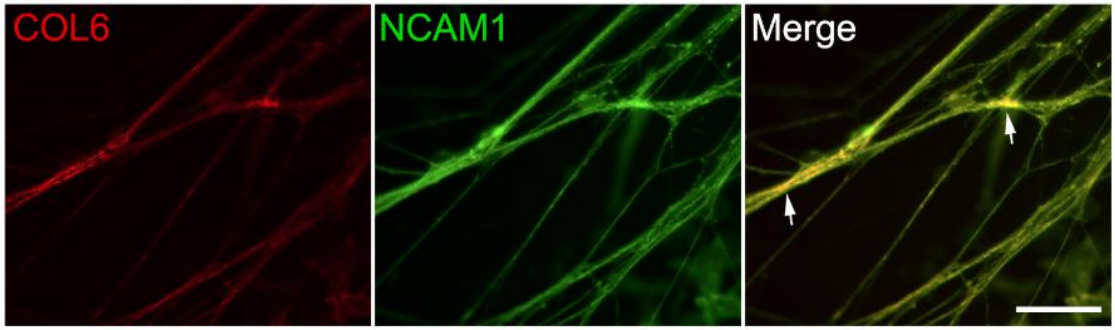

Additional Figure 6 Colocalization of COL6 and NCAM1.

DRG tissue blocks grow on the COL6-precoated substrate for 3 days, followed by immunofluorescence staining of COL6 and NCAM1, arrows indicate the colocalization of COL6 (red, stained by CY3) with NCAM1 (green, stained by Alexa Fluor 488). It should be noted that COL6 coating on the bottom creates serious background fluorescence by COL6 immunofluorescence staining, only the nerve bundles hanging close to the DRG tissue block can produce low background COL6 fluorescence image. Scale bar: 20 μm. This experiment has been repeated twice. COL6: Collagen VI; NCAM1: neural cell adhesion molecule 1.

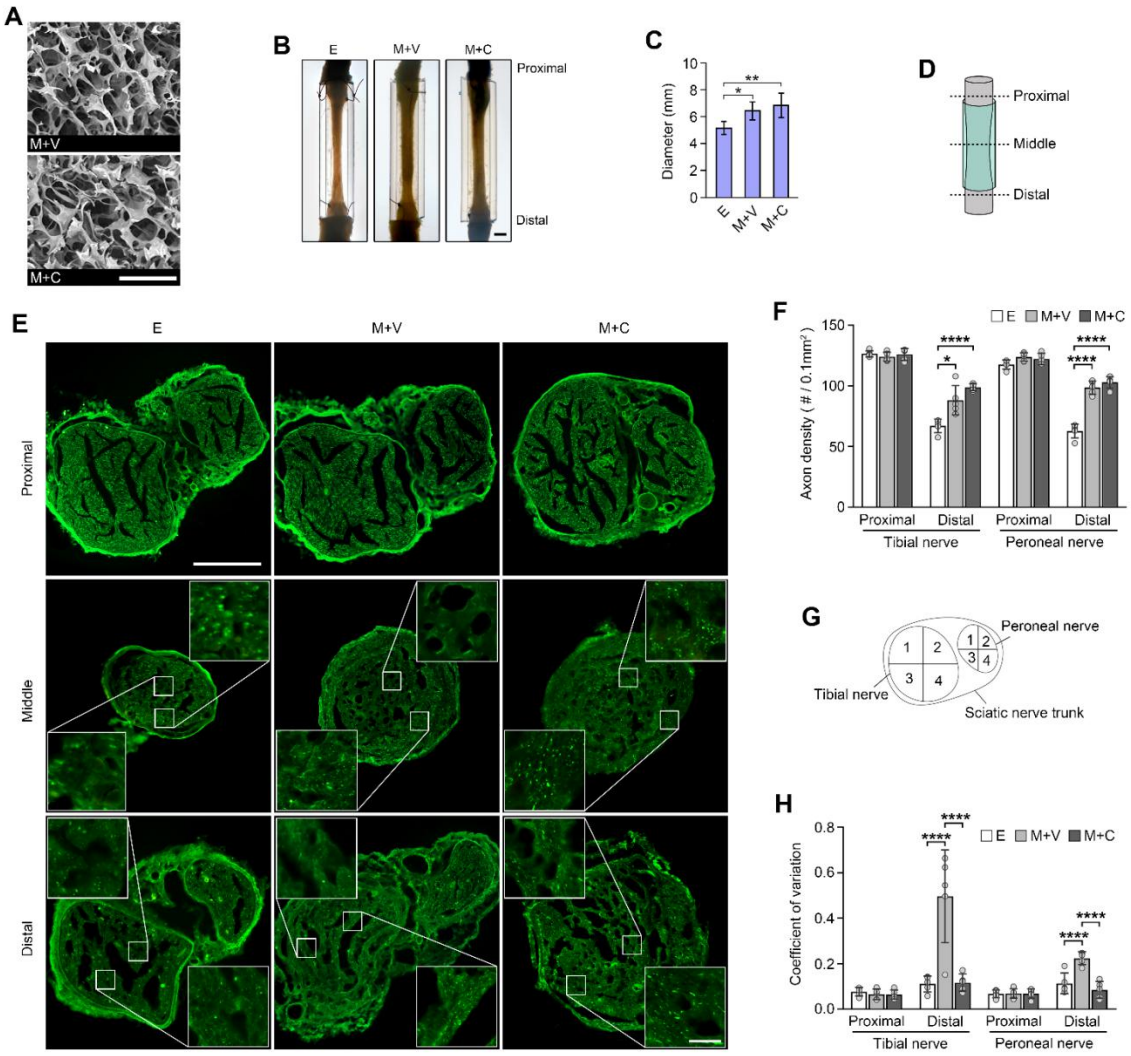

Additional Figure 7 COL6 improves the uniformity of regenerated axon distribution in the distal nerve trunk.

(A) Scanning electron microscopy of different hydrogel structures in the silicone catheters,which shows a porous structure of the M + V hydrogel similar to that of the M + V hydrogel. (B) After 8 weeks of regeneration, nerve stumps were connected by regenerated tissue in the catheter. The M + C group shows the largest diameter of regenerated nerve. (C) Histogram shows that the silicone catheter filled with hydrogel (M + V and M + C groups) resulted in a larger diameter of regenerated nerve tissue than did the empty catheter (E) (n = 5, **P* = 0.0314, ***P* = 0.0051, one-way analysis of variance followed by Tukey's multiple comparison tests). (D) Schematic of proximal, middle and distal cross sections. (E) Fluorescence microscopy of sciatic nerve cross sections indicated in D. The regenerated axons are only evenly distributed throughout the entire segment in the M + C group but not in the E and M + V groups. NF200 immunofluorescence-labeled axons were presented as light green dots (stained by Alexa Fluor 488). (F) Axon densities of the tibial nerve and peroneal nerve at proximal and distal cross sections are calculated and compared among different groups (n = 5, **P* = 0.0028, *****P* < 0.0001, one-way analysis of variance followed by Tukey's multiple comparison tests). (G) Schematic of quadrant division of tibial nerve and peroneal nerve in the sciatic nerve trunk. (H) Axon densities in

each quadrant were calculated. Histogram shows the coefficient of variation of axon densities in different groups (n = 5, ****$P < 0.0001$, one-way analysis of variance followed by Tukey's multiple comparison tests). Scale bars:100 μm (A), 8 mm (B), 400 μm (E) and 40 μm in the enlarged part of E. COL6: Collagen VI; E: empty; M + C: Matrigel + COL6; M + V: Matrigel + Vehicle.

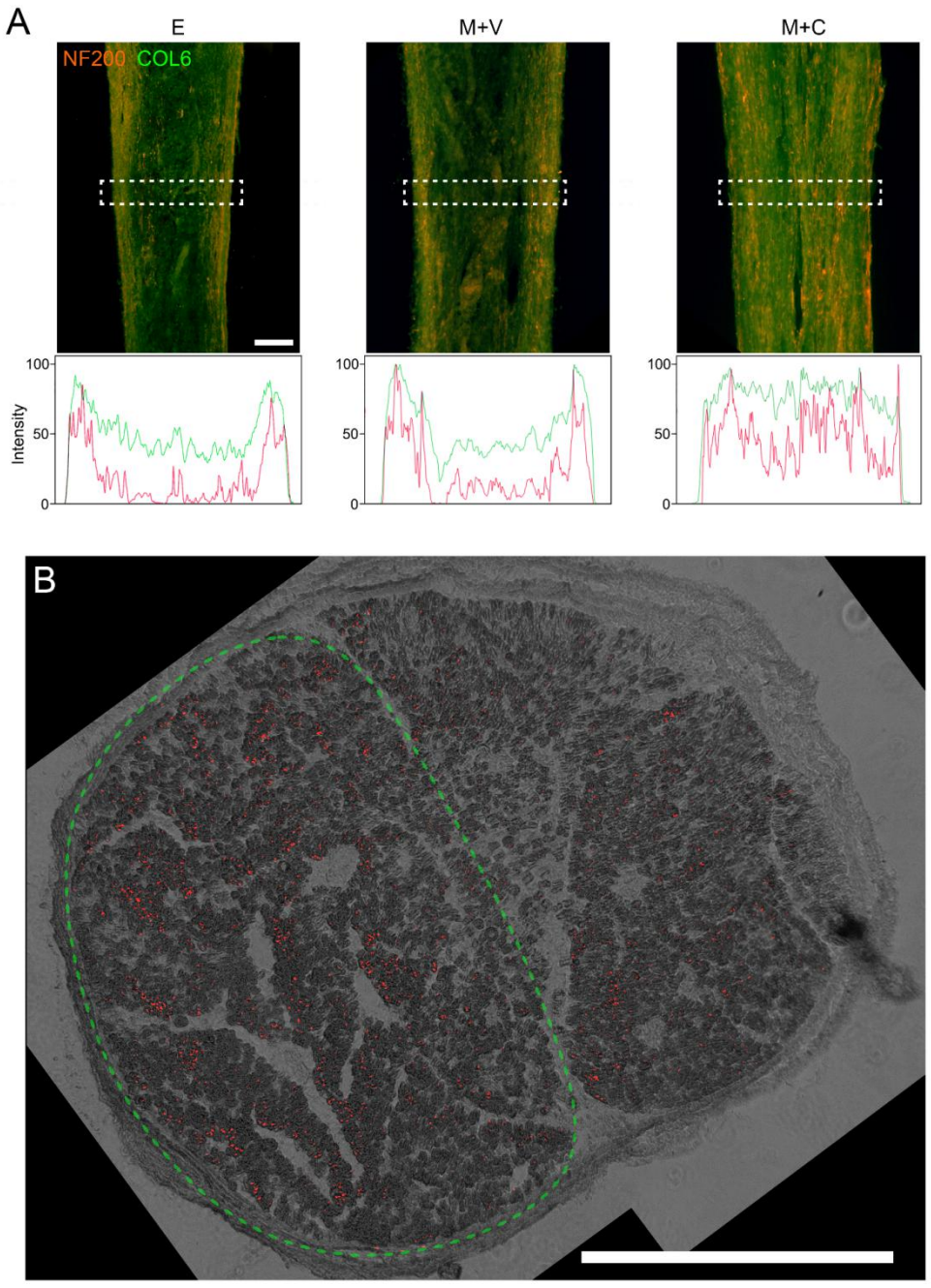

Additional Figure 8 Distribution patterns of NF200 and COL6 in the regenerated nerve tissues.
(A) Upper panel, representative images of NF200 (red, stained by Cy3) and COL6 (green, stained by Alexa Fluor 488) expression in regenerated sciatic nerve after 2 weeks repairing. The fluorescence signals of NF200 and COL6 are laterally distributed in the E and M + V groups, while the M + C group shows the uniform fluorescent signals of NF200 and COL6. Lower panel, Image Lab™ (version 6.0) software is used to analyse the fluorescence distribution pattern of the ROI (rectangle) above. x-axis represents the transverse span of the nerve within the white rectangle. (B) Representative image of sciatic nerve cross-section showing the retrograde fluorescence tracing on the tibial nerve tract in the M + V group. The green dotted line marks the region of tibial nerve tract; the red dots indicate the fluorescence positive axons. Scale bars: 200 μm (A), 400 μm (B). COL6: Collagen VI; E: empty; M +

V: Matrigel + Vehicle; M + C: Matrigel + COL6; NF200: Neurofilament 200; ROI: region of interest.